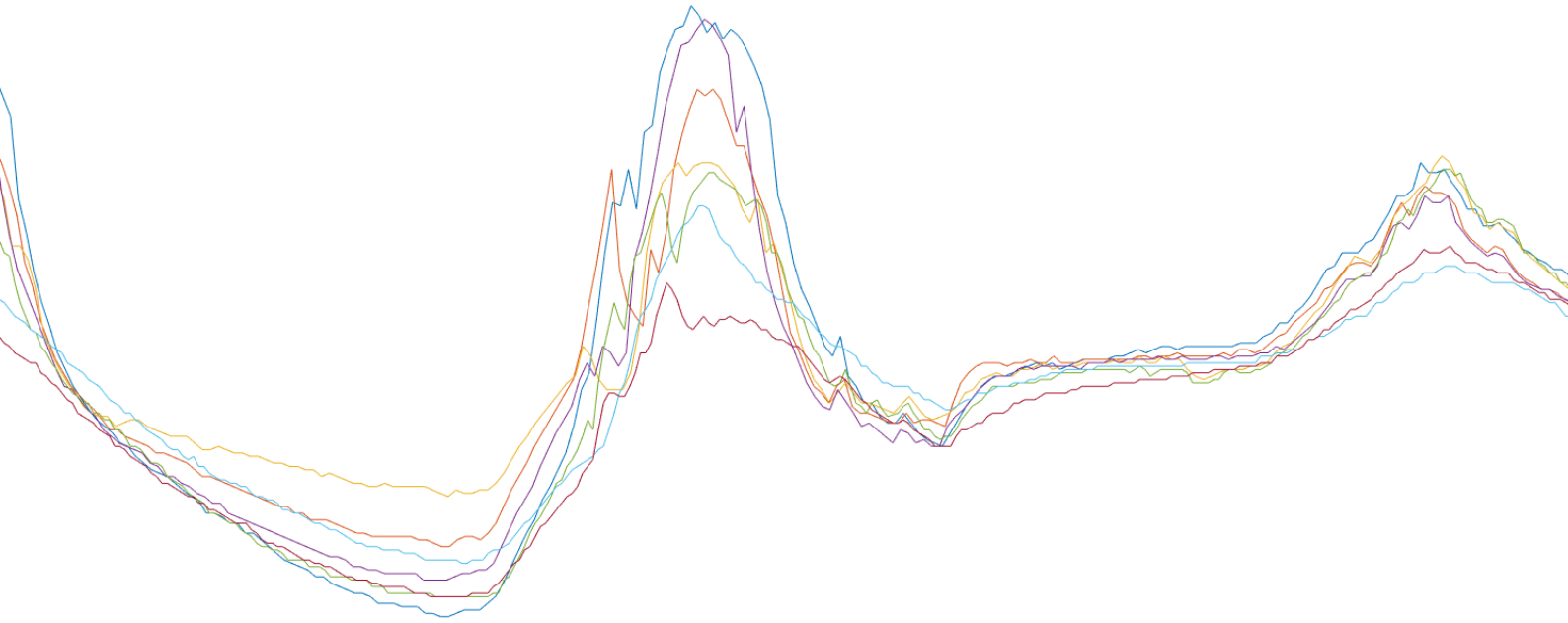
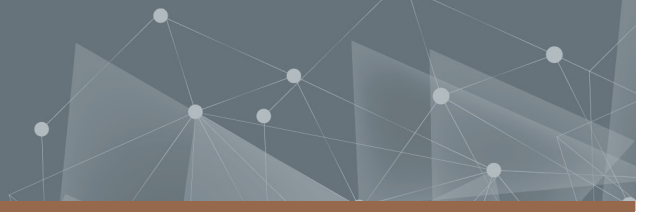




CHALMERS
UNIVERSITY OF TECHNOLOGY



Creating Road Surface Temperature Forecasts to Increase Bicycle Path Safety

Master's Thesis in Master Programs Product Development and System, Control and Mechatronics

VIKTORIA BOGREN

TINA MOSTAFAVI

Department of Electrical Engineering
CHALMERS UNIVERSITY OF TECHNOLOGY
Gothenburg, Sweden 2020

MASTER'S THESIS 2020

Creating Road Surface Temperature Forecasts to Increase Bicycle Path Safety

VIKTORIA BOGREN
TINA MOSTAFAVI



CHALMERS
UNIVERSITY OF TECHNOLOGY

Department of Electrical Engineering
Division of Systems and Control
CHALMERS UNIVERSITY OF TECHNOLOGY
Gothenburg, Sweden 2020
www.chalmers.se

Creating Road Surface Temperature Forecasts to Increase Bicycle Path Safety
VIKTORIA BOGREN
TINA MOSTAFAVI

© VIKTORIA BOGREN, TINA MOSTAFAVI, 2020.

Supervisor: Torbjörn Gustavsson, Klimator AB
Examiner: Jonas Fredriksson, Department of Electrical Engineering

Master's Thesis 2020
Department of Electrical Engineering
Division of Systems and Control
Chalmers University of Technology
SE-412 96 Gothenburg
Telephone +46 31 772 1000

Typeset in L^AT_EX
Printed by Chalmers Reproservice
Gothenburg, Sweden 2020

Creating Road Surface Temperature Forecasts to Increase Bicycle Path Safety
VIKTORIA BOGREN, TINA MOSTAFAVI
Department of Electrical Engineering
Chalmers University of Technology

Abstract

As a reaction to the United Nations' Sustainable development goals regarding active transportation, the need for increased road safety has expanded to bicycle paths. For car-borne roads, safe transportation has been increased by using tools that predict road slips, leading to improved road maintenance, anti-slip control, and warning systems. Currently, there are no similar tools for bicycle paths. One of the tools used for car-borne roads to improve road maintenance, is Road Station Information (RSI), a tool predicting slip that suggests how road maintenance can be optimized. One part of the RSI solution is a climate model forecasting road surface temperature on car-borne roads. This master's thesis aims to modify the existing climate model for car-borne roads, to predict the road surface temperatures on bicycle paths, around weather stations, to improve road maintenance and ensure safer active transportation. The project's method was to find differences between car-borne roads and bicycle paths and modify the climate model accordingly. The modifications to the climate model were made in two phases. The first phase included modifying the climate model parameters individually on a test data set to isolate how the parameters affect the road surface temperature forecast. The parameters modified were the parameter affecting shadows on the surface, called sky view factor (SVF), traffic amount, the thickness of the materials of the road surface, and road heat conductivity (RHC) of the surface. The second phase included validation of the results from the first phase, by modifying the parameters together and testing the modifications on a more extensive data set. The forecasts created were compared against measured values from Hede stations set up in a test area in Jönköping. The results showed that the parameters SVF and RHC affected the accuracy of the forecasts the most. The master's thesis concludes that the climate model for car-borne roads works well on bicycle paths in terms of accuracy. However, when comparing the results for bicycle paths with those for car-borne roads, it becomes apparent that the climate model can be improved for bicycle paths. The measures to be taken depend on which temperatures are considered critical and the accuracy required for bicycle paths. Overall, based on the results, it is recommended to develop a better method for calculating SVF for bicycle paths and to test lower values for RHC on bicycle paths.

Keywords: road surface temperature, climatology, climate model, forecast, road maintenance, slip, bicycle paths, weather station

Acknowledgements

We would like to take the opportunity to acknowledge and express our greatest gratitude to those who have supported and encouraged us throughout the project. Firstly, we would like to thank our examiner at Chalmers University of Technology Jonas Fredriksson, who has consistently supported us throughout the project, with valuable points as well as helpful insights and recommendations. Secondly, we would also like to take the opportunity to thank our supervisor Torbjörn Gustavsson and the employees Esben Almkvist and Peter Hagberg at Klimator AB for the great support regarding the Climate model and providing knowledgeable lectures. Finally, we would like to express our gratitude towards our families and friends who have consistently been supporting us throughout our time at Chalmers.

Viktoria Bogren, Tina Mostafavi, Gothenburg, May 2020

Contents

List of Figures	xi
List of Tables	xv
1 Introduction	1
1.1 Background	1
1.2 Aim	2
1.3 Specification of issues under investigation	2
1.4 Delimitations	2
2 Theory	5
2.1 Climatology and meteorology	5
2.1.1 Road climate and weather	6
2.1.2 Microclimate and local climate	9
2.1.3 Topography and topoclimates	10
2.2 The climate model for car-borne roads	11
2.2.1 The energy balance for a surface	12
2.2.2 Environmental factors affecting the energy balance	15
2.2.3 The process of the climate model when creating road surface temperature forecasts	19
2.3 Research regarding differences between car-borne roads and bicycle paths	21
2.3.1 Construction of car-borne roads and bicycle paths	21
2.3.2 Local differences affecting the climate model	22
2.4 Evaluation tools	24
3 Methodology	27
3.1 Installing Hede stations	27
3.1.1 Positioning of the Hede stations	27
3.1.2 The mounting process	31
3.2 Modification of the climate model	33
3.2.1 Setting up the testing environment and defining parameters	33
3.2.2 Testing SVF	35
3.2.3 Testing traffic amount	38
3.2.4 Testing Asphalt and underlying layer thickness	39
3.2.5 Testing RHC	39
3.2.6 Evaluating the testing phase and validating	40

4	Results	47
4.1	Differences between car-borne roads and bicycle paths	47
4.2	Plots from the testing phase	49
4.3	Tables and confusion matrices from the testing phase	55
4.4	Confusion matrices from the testing phase	64
4.5	Plots, tables, and confusion matrices from the validation phase	68
5	Discussion	71
5.1	Analyzing the results from the testing phase	71
5.1.1	Analyzing traffic amount	72
5.1.2	Analyzing thickness of the asphalt and underlying layers	73
5.1.3	Analyzing SVF	73
5.1.4	Analyzing road heat conductivity	75
5.2	Analyzing the results from the validation phase	76
5.3	Evaluation of the method	78
6	Conclusion and recommendations	81
6.1	Conclusion	81
6.2	Future work and recommendations	82
A	Appendix 1	I

List of Figures

2.1	The figure illustrates the differences in temperature variation between clear and cloudy days and nights. The picture to the left illustrates the air temperature during a clear day and night, and the picture to the right illustrates the air temperature during a cloudy day and night. The authors' own illustration.	7
2.2	The figure illustrates how the relation between air temperature and dew point leads different scenarios where evaporation, condensation and sublimation occur. The authors' own illustration.	8
2.3	A cross-section of a valley where a cold air lake emerge when cold air is formed near the ground. The authors' own illustration.	11
2.4	The figure illustrates the energy balance of the surface during a typical night. The authors' own illustration.	14
2.5	The figure illustrates the energy balance of the surface during a typical day. The author's own illustration.	15
2.6	Illustration of solar position for vernal equinox, summer and winter solicit. The horizontal angles are illustrated by the boxes and represents objects that hinder direct sunlight. The authors' own illustration. 16	16
2.7	The figure is a rough illustration of the iterative process of the algorithm. The gray dashed line illustrates the iteration of the energy balance to calculated a road surface temperature. The vertical dotted red line marks the start of the forecast, and the bold red dot shows the actual value measured by RWIS. The authors' illustration.	20
2.8	The figure is an illustration of how the measured value from RWIS at the start of the forecast, is relaxed together with the forecasts from SHMI. The red dotted line marked the start of the forecast. The authors' own illustration.	21
2.9	The scenarios of a binary confusion matrix and the rates that will be calculated in this project. Note that Σ Positive and Σ Negative is the summations of when the actual values are positive or negative.	25
3.1	A map showing how the stations were placed in Jönköping.	28
3.2	Pictures showing the surrounding of Hede station 1.	28
3.3	Pictures showing the surrounding of Hede station 2.	29
3.4	Pictures showing the surrounding of Hede station 3.	30
3.5	Pictures showing the surrounding of Hede station 4.	30

3.6	Pictures showing the hole and placement for the cable and its plastic cover.	31
3.7	Pictures showing how the surface temperature sensor was placed into the asphalt.	32
3.8	Pictures showing a fully mounted Hede station.	32
3.9	A map showing the locations of the Hede stations and RWIS measuring local weather data for this thesis	34
3.10	The figures shows how the sectors used when calculating horizontal angles are divided around the Hede stations. The sectors are illustrated with sectioned light gray circles. The orientations of the pictures are noted with compasses in the lower right corners.	36
3.11	The figure illustrates how the horizontal angles were calculated with tangent for the different objects using their height and distance to the stations. In the figure HA stands for horizontal angle, d stands for distance between station and object, and h stands for height of the object.	37
3.12	A plot showing the forecasts for surface temperature made with modifications on SVF for Hede 4. The plot illustrates the dip that occurs in the middle of the day with SVF manually calculated.	41
3.13	The figure illustrated the sections around Hede 4 after refinement. The stretched lines illustrates the sections added during refinement.	42
4.1	Measured values from all Hede stations and RWIS.	49
4.2	Plot with forecasts where the SVF parameter is modified around Hede station 1.	50
4.3	Plot with forecasts where the SVF parameter is modified around Hede station 2.	50
4.4	Plot with forecasts where the SVF parameter is modified around Hede station 3.	51
4.5	Plot with forecasts where the SVF parameter is modified around Hede station 4.	51
4.6	Plot with forecasts where the traffic amount parameter is modified around Hede 1.	52
4.7	Plot with forecasts where the parameters thickness of the asphalt and the underlying layers are modified around Hede station 1.	52
4.8	Plot with forecasts where the RHC parameter is modified around Hede station 1.	53
4.9	Plot with forecasts where the SVF parameter is modified around RWIS 653.	53
4.10	Plot with forecasts where the traffic amount parameter is modified around RWIS 653.	54
4.11	Plot with forecasts where the parameters thickness of the asphalt and the underlying layers are modified around RWIS 653.	54
4.12	Plot with forecasts where the RHC parameter is modified around RWIS 653.	55

4.13	The figures show the confusion matrices for when the RHC parameter was modified on the test data set around the Hede stations.	65
4.14	The figures show the confusion matrices for when the RHC parameter was modified on the test data set around RWIS.	66
4.15	The figures show the confusion matrices for when the SVF parameter was modified on the test data set around Hede.	67
4.16	The figures show the confusion matrices for when the SVF parameter was modified on the test data set around RWIS.	67
4.17	Plot with measured values and 4-hour forecasts where the SVF and RHC parameters has been modified around Hede 1. The plots shows measured values and forecasts made on February 27-March 27.	68
4.18	Plot with measured values and 4-hour forecasts where the SVF and RHC parameters has been modified around RWIS 653. The plots shows measured values and forecasts made on February 27-March 27.	68
4.19	The figures show the confusion matrices for when the default and modified values were used on the validation data set around the Hede stations. In the matrices, the green values represent when the forecasts and measured values agree with each other; the yellow values represent the false negatives, and the red value represents the false positives. In the matrices, different rates are calculated based on the formulas in figure 2.9	69
4.20	The figures show the confusion matrices for when the default and modified values were used on the validation data set around the RWIS. In the matrices, the green values represent when the forecasts and measured values agree with each other; the yellow values represent the false negatives, and the red value represents the false positives. In the matrices, different rates are calculated based on the formulas in figure 2.9	69

List of Tables

2.1	The parameters in the energy balance for the surface.	12
2.2	Heat conductivity for materials that are normally used to construct roads.	17
2.3	The table shows the sources for the variable input parameters for the algorithm.	19
2.4	The table shows the different weather data that is measured for Hede stations and RWIS. The table only shows weather data that is used in the climate model to calculate surface temperature, and does not include other data.	23
3.1	The average SVF values for each station.	38
3.2	The estimated ÅDT for Hede stations and actual ÅDT for RWIS, used in second modification for traffic amount.	39
3.3	The average SVFs for manually calculated SVF for all Hede and the manually calculated and refined SVF for Hede station 1 and 4.	42
3.4	The table presents the MAE and RMSE for the forecasts where the SVF parameter was modified, around the Hede stations.	43
3.5	The table presents the MAE and RMSE for the forecasts where the traffic amount parameter was modified, around the Hede stations.	43
3.6	The table presents the MAE and RMSE for the forecasts where the asphalt thickness parameter was modified, around the Hede stations.	44
3.7	The table presents the MAE and RMSE for the forecasts where the RHC parameter was modified, around the Hede stations.	44
3.8	The table presents the MAE and RMSE for the forecasts where the traffic amount parameter was modified, around the Hede stations. The forecasts used when calculating the errors were 8-hour forecasts made on the whole test data set (February 27-29 and March 7-9). In the table the smallest errors for each station are highlighted.	45
4.1	The estimated ÅDT for Hede stations and actual ÅDT for RWIS, used in second modification for traffic amount.	48
4.2	The table shows the different weather data that is measured for Hede stations and RWIS. The table only shows weather data that is used in the climate model to calculate surface temperature, and does not include other data.	48
4.3	The table presents the MAE for the forecasts where the SVF parameter was modified around the Hede stations.	56

4.4	The table presents the RMSE for the forecasts where the SVF parameter was modified, around the Hede stations.	56
4.5	The table presents the MAE for the forecasts where the SVF parameter was modified, around RWIS.	57
4.6	The table presents the RMSE for the forecasts where the SVF parameter was modified, around RWIS.	57
4.7	The table presents the MAE for the forecasts where the traffic amount parameter was modified, around the Hede stations.	58
4.8	The table presents the RMSE for the forecasts where the traffic amount parameter was modified, around the Hede stations.	58
4.9	The table presents the MAE for the forecasts where the traffic amount parameter was modified, around RWIS.	59
4.10	The table presents the RMSE for the forecasts where the traffic amount parameter was modified, around RWIS.	59
4.11	The table presents the MAE for the forecasts where the asphalt and underlying layer thickness parameter was modified, around the Hede stations.	60
4.12	The table presents the RMSE for the forecasts where the asphalt and underlying layer thickness parameter was modified, around the Hede stations.	60
4.13	The table presents the MAE for the forecasts where the asphalt and underlying layer thickness parameter was modified, around RWIS.	61
4.14	The table presents the RMSE for the forecasts where the asphalt and underlying layer thickness parameter was modified, around RWIS.	61
4.15	The table presents the MAE for the forecasts where the RHC parameter was modified, around the Hede stations.	62
4.16	The table presents the RMSE for the forecasts where the RHC parameter was modified, around the Hede stations.	62
4.17	The table presents the MAE for the forecasts where the RHC parameter was modified, around RWIS.	63
4.18	The table presents the RMSE for the forecasts where the RHC parameter was modified, around RWIS.	63
4.19	The table presents the MAE and RMSE for the forecasts where the SVF parameter was modified, around the Hede stations, during sunrise. The forecasts used when calculating the errors were 4-hour forecasts made on the whole test data set (February 27-29 and March 7-9). The calculations are made for the time interval 07:00-11:00 to show the effects of the SVF parameter during sunrise. In the table the smallest errors for each station are highlighted.	64
4.20	The table presents MAE and RMSE for forecasts made on Hede stations where the SVF and RHC parameters were modified, and for when default values were used on all parameters. The forecasts used when calculating the errors were 4-hour forecasts made on the validation data set (February 27-March 27). The calculations were made on all temperatures, the temperature interval 5 to -5°C , and the temperature interval 2 to -2°C	70

4.21	The table presents MAE and RMSE for forecasts made on RWIS stations where the SVF and RHC parameters were modified, and for when default values were used on all parameters. The forecasts used when calculating the errors were 4-hour forecasts made on the validation data set (February 27-March 27). The calculations were made on all temperatures, the temperature interval 5 to -5°C , and the temperature interval 2 to -2°C	70
------	---	----

1

Introduction

In this chapter, the foundation of the project is described through the background description, aim formulation, the definition of limitations, and specification of issues under investigation including the research questions of the project.

1.1 Background

With the grand challenge climate change in mind, it lies in the interest of engineers to contribute to a sustainable society. There are several ways to operate, and one goal highlighted in the UN's Sustainable development goals United Nations (2020) and by EU European Commission (2020) is to provide access to safe, affordable, accessible, and sustainable transport systems, and improved road safety. A potential way for sustainable and active transportation is to increase the use of bicycles. Today, this mode of transportation is not safe during winter due to a lack of information regarding the bicycle path network condition, resulting in poor road maintenance. According to the Swedish Public Health Authority, the risk for single bicycle accidents could decrease by up to 25% as a result of improved road maintenance during winter, which results in higher safety and therefore encourages people to increase their use of bicycles (Faskunger, 2008, p. 28).

Systems are running to ensure safe transportation for car-borne traffic, in terms of maintenance, anti-slip control, and warning systems. One of these is the state-of-art system, Road Status Information (RSI), developed by Klimator AB. RSI is a software designed to detect slip, deliver forecasts, and suggest safety measures to ensure a non-slip road for cars Klimator AB (2020). One part of the RSI solution the climate model based on the open-source software model, Model of the Environment and Temperature of Roads (METRo). The climate model predicts road temperature and road conditions, using information from Road Weather Information Stations (RWIS), topology, weather forecast, and road treatment actions. As for today, there are no corresponding climate models for bicycle paths on the market.

As a reaction to the UN's Sustainable development goals regarding active transportation, the need for increased and improved road maintenance has expanded to bicycle paths. A step towards improving road maintenance and increase safety on bicycle paths is to transfer the knowledge about car-borne road maintenance software

models to bicycle paths.

1.2 Aim

This master's thesis aims to modify the existing climate model from RSI for car-borne roads, to predict the road surface temperatures on bicycle paths, around weather stations, to improve road maintenance and ensure safer active transportation.

1.3 Specification of issues under investigation

The following research questions have been developed, with limitations in regard, to ensure that the aim is fulfilled.

RQ.1 What are the differences between car-borne roads and bicycle paths, e.g., in terms of road construction and amount of traffic?

RQ.2 What modifications in the climate model lead to more accurate forecasts on an area surrounding Hede stations installed on bicycle paths, with measured data from the Hede stations as a reference?

RQ.3 Do the same modifications apply for car-borne roads with RWIS as a reference?

1.4 Delimitations

Delimitations have been established for the master's thesis based on the level of readiness and physical restrictions, such as resources and locations. The delimitations made for this master's thesis are described below.

- The purpose of the finished product is to proactively prevent road slip by providing forecasts and measures regarding road slip to contractors. This project is classified as an R&D-project and will, therefore, only concern forecasts for road surface temperature. Road slip will not be taken into account.
- The placement and distance between the sensors are essential to lower cost while optimizing the performance of model and ensure a complete bicycle path coverage. Due to the early phase in the development process, the placement optimization will not be taken into consideration in this project.
- The Hede stations will be mounted in specific locations decided by Klimator. The project will, therefore, only concern and analyze the results from these

selected areas, which also limits the type of bicycle paths and microclimates analyzed.

- Depending on which customer segment that is using the finished product, the need for precision of the forecast will vary. This project will not evaluate if the precision of the forecast is good enough for a specific customer. The project will only evaluate how the parameters affect the result and investigate if parameter modification can lead to a better result.

2

Theory

In this chapter, the theory needed to perform the thesis is presented throughout four sections. The first section, Climatology, and meteorology, describes central concepts such as weather, microclimate, and topography to create essential understanding for road climate. In the second section, The climate model for car-borne roads, the climate model which will be modified, and the algorithm creating forecasts, are explained. The second section does also include a detailed description of the energy balance. In the third section, Differences between bicycle paths and car-borne roads, research question one (RQ.1), is processed by listing differences, possibly leading to changes in the climate model. The last section, Evaluation tools, describes the tools used during evaluation to measure the accuracy and performance of the modified climate model.

2.1 Climatology and meteorology

Climatology is the study of conditions in the atmosphere above a specific area over a long period, typically 30 years. Meteorology is the study of weather conditions over a short period, typically a forecast for a few days. Meteorology is the science of clouds, rain, and wind. It studies air and water in terms of fluid mechanics and uses it to describe the weather. To define weather and create a weather forecast, local values provided by local weather stations and satellites, are used together with atmospheric evolution models. Climatology studies a series of meteorological data, to establish a significant mean value and can, therefore, explain irregularities and define different types of climate. When studying climate, geographical factors like the distribution of land and sea needs to be taken into consideration, Mayer (2020)

There are three types of climate frequently referred to, depending on the size of the area studied and the accuracy of the measurements. The three types of climate are macro-, local- and microclimate. According to Metlink (2020), these are relevant to study since the differences in climate can explain certain weather phenomena. Macroclimate is referring to larger areas with a low precision level of the measurements, such as the temperature in the south of Sweden, (Lindqvist et al., 1983, p. 13). The local climate is referring to a smaller area and has a higher precision compared to macroclimate. Factors that affect the local climate are topography, the number of buildings, and the amount of vegetation. Examples of local climates are

cities, forests, or valleys, (Lindqvist et al., 1983, p. 13). Microclimate refers to a small area with a high level of precision on the measurements. In microclimates, measurements shift within a couple of meters. When studying road climate, the microclimate distinguishes the air right above the road surface, the ground below, and the surface itself. When the microclimate of road segments are studied, it is called road climate (Lindqvist et al., 1983, p. 13). Just like the local climate, the microclimate is depending on the topography, which affects and steers the weather.

Both climatology and meteorology are needed to describe road climate, and thereby the road surface temperature. The weather, micro- and local climate, and local topography are central and recurring concepts connected to road climate, and will be describe in the following sections.

2.1.1 Road climate and weather

Weather explains the state of the atmosphere at a specific time for the weather variables air temperature, cloud, wind, precipitation, and humidity level, which affect the road climate. This section explains the relationship between road climate and weather and how the weather variables affect the road climate. Since the weather variables are needed to explain the road climate at specific locations, there is a network with sensors along car-borne roads in Sweden called Road Weather Information Stations (RWIS), collecting local weather data.

The driving force in all weather events is the shortwave radiation from the sun, which reaches the atmosphere and ground mainly as visible light. During the day, the solar radiation heats the ground, which in turn heats the air above. The air temperature, therefore, becomes warmer close to the road surface and cools down with increased height, according to Lindqvist et al. (1983).

According to Lindqvist et al. (1983), at night, when there is no shortwave radiation, heat leaves the ground as longwave radiation. The cold ground cools the air closest to the surface, and the air temperature can become warmer with increased height. The phenomenon when the temperature close to the surface is cooler than the temperature at around 2 meters above the surface, is called temperature inversion. When inversion occurs, the cold temperatures near the surface leads to an increased risk of precipitation freezing on the road. Inversion can only occur during windless nights.

As explained above, the air temperature varies with height, leading to different air temperatures being measured depending on the height of the measurement instrument. According to Peterson & Ringström (1977), the convention for road climate is to measure the temperature gradient from the surface up to 2 meters above the surface, which is what RWIS are set to. The relation between air temperature and surface temperature is a key factor when studying road climate and slip hazards since it has an impact on e.g., ice formation.

Clouds impact both shortwave and longwave radiation. During the daytime, the

incoming radiation from the sun and sky is partly reflected by the clouds. The radiation does, therefore, not reach the surface to the same extent, leading to lower air temperatures. During the night, the clouds hinder the longwave heat radiation from disappearing from the terrestrial layer, leading to higher temperatures during cloudy nights. According to Lindqvist et al. (1983), the cloudiness will also prevent the temperature from dropping as fast as during a clear night. This means that if it is cloudy, the difference in temperature between day and night will be small, around 1-2 ° C, and during a clear day and night, the temperature difference can become as big as 15-20 ° C. Cloud's equalizing effect on air temperature is illustrated in figure 2.1.

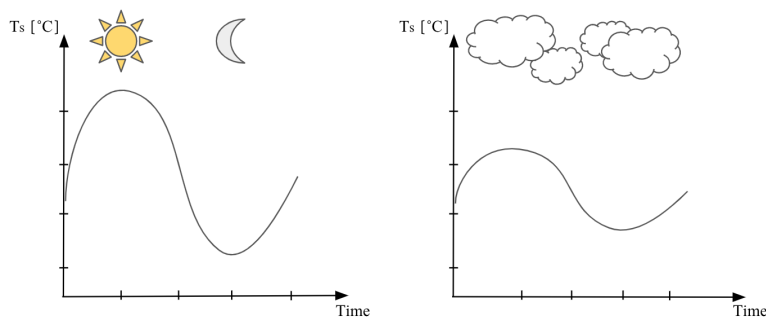


Figure 2.1: The figure illustrates the differences in temperature variation between clear and cloudy days and nights. The picture to the left illustrates the air temperature during a clear day and night, and the picture to the right illustrates the air temperature during a cloudy day and night. The authors' own illustration.

The wind is a result of nature striving to equalize pressure differences, where higher pressure differences, leads to stronger winds. When the wind is blowing, air masses with different temperatures are mixed, which affects the resulting air temperature. According to Lindqvist et al. (1983), turbulence mixes air from different locations and evens out the difference between the air temperature measured 2 meters above the surface, and the air temperature close to the surface. During the day, the equalization happens through wind mixing the air close to the surface with the colder air masses above. At nighttime, the opposite happens with wind mixing the air close to the surface with the warmer air masses above. A typical example of high-risk weather, described by Lindqvist et al. (1983) regarding road climate, is, therefore, the combination of windless and starry nights. During windless and starry nights, the air temperature drops fast due to the clear sky, and the temperature near the road surface is not evened out by the wind, leading to the risk of ice formation.

As described by Lindqvist et al. (1983) precipitation occurs when clouds rise, and water is released. The clouds are formed when humid air is forced upwards, and the air temperature drops. The water from the clouds is released as snow, which, if the temperature is above 0° C, reaches the ground as raindrops. The quantity of precipitation differs significantly depending on the topography, and can, therefore, vary in between nearby locations. For example, the quantities of precipitation are

2. Theory

often higher in high-lying areas. Regarding road climate, precipitation affects the amount of radiation absorbed by the road. Almkvist (2020) explains that when the surface is covered with snow or ice, more shortwave radiation is reflected, leading to less radiation being absorbed by the surface. Furthermore, Almkvist (2020) means that precipitation also affects the amount of water on the road surface. When water is freezing or melting, heat from the road is needed. As a result, the road temperature is usually preserved around the water's freezing point during the phase change. According to Almkvist (2020), the wind affects how much precipitation that stays on the road surface since it can speed up the drainage and drying process.

The relative humidity, together with the air temperature, determine the dew point. If the dew point is below 0°C , it is called the freezing point. The dew point is the temperature when the air is saturated for a given amount of water vapor in the air. Thus the dew point describes how much water the air can hold before it condenses/sublimates or evaporates, which affects the formation of dew, fog, and frost. Warmer air can contain more water vapor, Lindqvist et al. (1983). If the relative humidity is 100%, the dew point is equal to the measured air temperature. If the surface temperature is above 0°C , water vapor will precipitate as droplets at the dew point, so-called dew. This is called condensation. If the surface temperature is below 0°C , sublimation occurs instead. Sublimation is when ice crystals are formed on the road surface, so-called frost. Condensation/sublimation and evaporation are illustrated in figure 2.2. Greater differences between air temperature and surface temperature lead to a thicker dew or hoarfrost layer. Another factor affecting the thickness of the dew and hoarfrost layer is wind. Lindqvist et al. (1983) explains that the wind contains new masses of water vapor, which can be deposited during condensation/sublimation or evaporation. Thus hoarfrost layer created from sublimation is thinner when the wind is calm and thicker when the wind is stronger. If the droplets/ice crystals are formed in the air, fog/frost fog occurs.

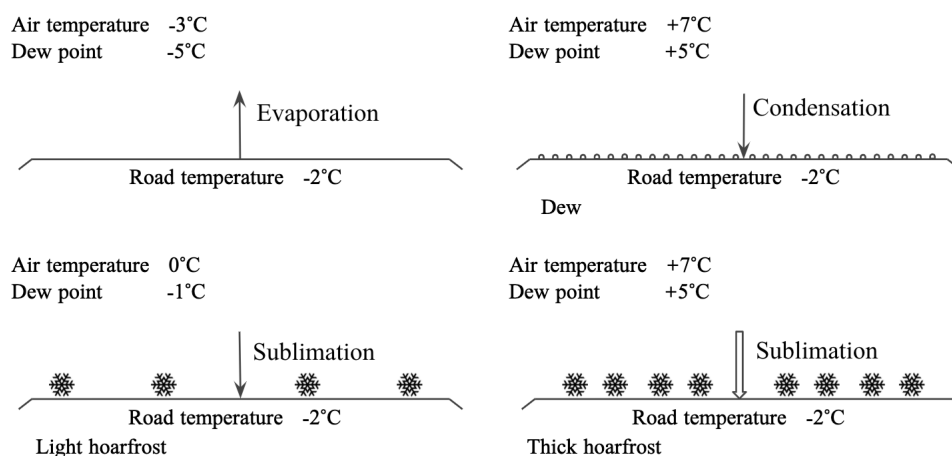


Figure 2.2: The figure illustrates how the relation between air temperature and dew point leads different scenarios where evaporation, condensation and sublimation occur. The authors' own illustration.

2.1.2 Microclimate and local climate

According to Lindqvist et al. (1983), the road climate is a type of microclimate and refers to a small area. It is distinguished by an area with high precision, regarding the weather variables such as surface and air temperature, precipitation, wind, and relative humidity. The microclimate is affected by surrounding factors such as nearby vegetation, the albedo of the surface, and the construction and heat conductivity of the ground. By studying the microclimate in road segments, the road climate can be described. There are different types of local climates that affect the microclimate, and thereby the road climate, which will be described in this section. According to Metlink (2020), the most common local climate types are city, rural, forest, and coastal, where a repeated pattern in the behavior of microclimate can be found. Note that the conditions in the microclimate can differ from the overall local climate; an example of this explained in this section is the so-called park cool island.

The microclimate in cities is usually a few degrees warmer compared to surrounding rural areas according to Peterson & Ringström (1977). This phenomenon is referred to as an urban heat island. A factor that contributes to urban heat islands is the lack of open areas. During the daytime, less shortwave radiation from the sun and sky is reflected to the atmosphere, due to the lack of exposed land surface. Instead, the radiation is absorbed by buildings and vegetation in the city, and heat is preserved in these objects. During the nighttime, there is a reduced heat loss in the street space. The longwave radiation is absorbed or reflected to the surface by obstructing surfaces such as buildings and other objects. There is also absorption and re-emission of longwave radiation due to air pollution in the urban atmosphere. According to Davéus (2016), the temperature difference between rural and city areas is usually more considerable during nighttime due to the reduced heat loss caused by the objects in the urban areas. Except for the lack of open areas, another factor is increased heat radiation caused by underlying heating systems, other energy use, industries, as well as an increased amount of traffic. The warmer temperatures in the urban areas lead to a decreased risk of ice formation on the roads compared to rural areas, especially during nighttime.

Davéus (2016) describes another microclimate phenomenon that can occur in a city area called park cool island. A park cool island is a park zone within the heat island where the temperature is significantly lower than in the surrounding city. A park cool island can, depending on the specific park and its regular daily pattern, either create a cool island during the day or a cool island during the night, depending on the park's properties. Park cool islands formed during daytime are usually formed in parks with high levels of vegetation and well-watered grass areas. The combination of shadows from trees and moisture from grass creates cooler parks in the day. During the night, the cooling process is slowed down by vegetation in these areas. When the park cool island is formed during nighttime, it usually occurs in dry city parks where the tree population is sparse. This is because an open flat surface leads to a faster cooling process during the night. Davéus (2016)

Coastal microclimate, or microclimate near large water bodies, is affected both by the land area and the water according to Metlink (2020). The water holds an even temperature compared to land due to the thermal properties of water. It takes a long time for water to heat up or cool down, which leads to cooler air temperatures during summer and warmer temperatures during winter. As a consequence of the water body being warmer and not freezing during winter, the level of moisture in the air is increased. The increased levels of moisture, combined with low air temperature, lead to a higher risk for sublimation and, in its turn, the formation of black ice and hoarfrost. Metlink (2020) explains that if the night is clear and calm, a more significant difference between air temperature and the surface temperature will occur. The great temperature difference leads to a thicker hoarfrost layer. If the water body is of a smaller size, the water body will freeze during winter. As a result of this, the highest risk for black ice and hoarfrost occurs during autumn when the moisture level is higher in the air.

The microclimate for forest areas depends on the homogeneity of the forest. In homogeneous forests, the temperature difference between day and night is small. During the day, vegetation in the homogeneous forest hinders shortwave radiation from reaching the surface. The decreased amount of absorbed shortwave radiation results in a lower air and surface temperature in such areas. During the night, longwave radiation from the ground is inhibited by the vegetation. If the forest alters between glade and dense areas, it is no longer referred to as a homogeneous forest. In such areas, the vegetation in the dense areas creates shadows on the glade areas, which hinders shortwave radiation from being absorbed during the day. This leads to ice remaining longer on these shadowed areas. An example of this is when a road goes through a forest. The width of the road, in correlation to the forest population height, is of the highest importance regarding the risk for ice formation. If the road is narrow, the vegetation emits longwave heat radiation that gets absorbed by the road and counteracts ice formation. The surface and air temperatures are, therefore, relatively high during the night in such cases. If the road is somewhat broader cut-out, the longwave radiation from the vegetation is small, and the risk for ice formation increases, Lindqvist et al. (1983).

2.1.3 Topography and topoclimates

According to Peterson & Ringström (1977), the surrounding topography does, for example, affect the amount of shortwave radiation that reaches the ground, and the emergence of cold-air lakes, which affect the road climate. The topography is most often used when describing the local difference in altitudes, such as valleys or hills. The different types of topoclimates described in this section are the upland area, valley, and slopes.

An upland area is described by Metlink (2020) as an area on a height where the surrounding topography is considerably lower. In an upland area, the air temperature, cloudiness, and precipitations are affected, and the air temperature is typically lower in upland areas. According to Lindqvist et al. (1983) the temperature drops at a rate of $0,5^{\circ}\text{C}$ to 1°C per 100 meters. The upland also contributes to the

formation of clouds, as a result of humid air rising and being cooled down, which can lead to increased precipitation in upland areas.

In valleys, where the surrounding topography is higher, the risk for the emergence of cold-air lakes occurs. As a result of cold air being heavier than warm air, cold-air lakes emerge when the cold air slides down and settles at the bottom of the valley, see figure 2.3. The risk is higher during clear and windless nights when cold air is formed near the ground. The temperature can be up to $2 - 6$ ° C lower in valleys where cold-air lakes emerge, which increases the risk for dew and hoarfrost formation, Lindqvist et al. (1983).

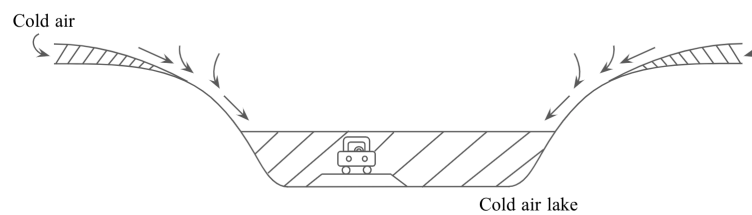


Figure 2.3: A cross-section of a valley where a cold air lake emerge when cold air is formed near the ground. The authors' own illustration.

Slopes affect the amount of shortwave radiation that reaches the surface. As explained by Lindqvist et al. (1983), the amount of radiation absorbed by the ground will either be increased or reduced, depending on how steep the slope is and which direction the slope is facing. The direction of the slope and its correlation to the sun's position determine if the slope is shaded or sunny. A shaded slope is colder and more humid than the surrounding environment. Snow and ice do, therefore, stay longer in such slopes, Lindqvist et al. (1983). The two cardinal directions that have the greatest impact, regarding shade and sun are north and south. A slope facing north may receive direct sunlight during early mornings and late evenings, depending on the time of the year. During winter, a north slope may not receive any direct sunlight at all. As a result, a slope facing north will receive a reduced amount of solar radiation compared to a flat surface. On the other hand, if a slope is facing south, the amount of solar radiation may increase significantly. For example, a slope facing south, with a slope angle of 20 ° can receive double the amount of solar radiation, compared to a flat surface, in January, (Geiger et al., 1995, p. 328). According to Geiger et al. (1995), slopes facing east or west mostly receive solar radiation in the forenoon and afternoon, respectively.

2.2 The climate model for car-borne roads

In this section, the climate model, and how it is designed for car-borne roads, is explained. The climate model contains an energy balance and a water model, and uses collected data, from both RWIS and weather forecast database SMHI, to fore-

cast road slip. The water model is not needed to forecast road temperature alone. Since this project is demarcated to only examine road temperature forecasts, the water model will not be further described. Instead, the energy balance, its parameters, and how the energy balance is affected by the surrounding environment will be explained. Furthermore, the section will also include a description of the algorithm in the climate model and its process, and how it uses the energy balance to forecast road temperature.

In this section, two types of parameters are described. The first is directly used in the energy balance, and the second is used in the algorithm. The parameters directly used in the energy balance will be described in section 2.2.1, and can be recognized by starting with the letter Q in their abbreviation. The parameters used in the climate model are environmental factors, affecting the parameters in the energy balance. The parameters that can be adjusted in the climate model will be described in section 2.2.2.

2.2.1 The energy balance for a surface

According to Peterson & Ringström (1977), the energy balance for a surface describes how radiation and heat between the surface, the air layer above and the ground below are exchanged. The energy balance for a surface is used in the climate model to estimate the road surface temperature, which is a part of the road climate.

$$Q_S - Q_R + Q_{L\downarrow} - Q_{L\uparrow} = \pm Q_H \pm Q_G \pm Q_{EC} \pm Q_{MF} + Q_A \quad (2.1)$$

The parameters in the energy balance are the radiation from the sun and sky (Q_S), the radiation reflected by the surface (Q_R), heat radiation from the atmosphere ($Q_{L\downarrow}$), heat radiation from the surface ($Q_{L\uparrow}$), heat exchange with the ground (Q_G), heat exchange with the air (Q_H), latent heat from evaporation or condensation (Q_{EC}), the heat needed during melting and freezing (Q_{MF}) and heat from traffic (Q_A), see table 2.1, Peterson & Ringström (1977)

Table 2.1: The parameters in the energy balance for the surface.

Energy balance parameter	Description
Q_S	The radiation from the sun and sky
Q_R	The radiation reflected by the surface
$Q_{L\downarrow}$	Heat radiation from the atmosphere
$Q_{L\uparrow}$	Heat radiation from the surface
Q_G	Heat exchange with the ground
Q_H	Heat exchange with the air
Q_{EC}	Latent heat from evaporation or condensation
Q_{MF}	Heat needed during melting or freezing
Q_A	Heat from traffic

The radiation from the sun and sky, Q_S , supplies the surface with energy and is characterized as shortwave. The shortwave radiation has a wavelength between 0,1-

0,4 micrometers and contains more energy than longwave radiation according to SMHI (2020). Since it contains more energy, shortwave radiation results in a faster heating process of the surface, compared to longwave radiation. Some radiation from the sun and sky is reflected, Q_R , and does not provide the surface with energy. According to Almkvist (2020), the amount of radiation that is reflected depends on the shortwave albedo of the road (A_S). A darker road has smaller albedo, which leads to less reflection and thus more energy being absorbed by the surface. A shortwave albedo of 0.1 means that the surface absorbs around 90% of the radiation from the sun.

Peterson & Ringström (1977) explains that longwave heat radiation is exchanged between the surface and the atmosphere. The surface radiates heat to the atmosphere, $Q_{L\uparrow}$, and the atmosphere radiates heat to the surface, $Q_{L\downarrow}$, e.g., heat radiation from air molecules, cloud, trees, and nearby objects. Some of the longwave heat radiation from the atmosphere, $Q_{L\downarrow}$, is reflected by the surface. According to Almkvist (2020), the amount of longwave radiation reflected depends on the longwave albedo (A_L). The longwave albedo is typically smaller than the shortwave albedo, meaning that the surface reflects less of the longwave radiation compared to shortwave radiation. The heat radiated from the surface is described by

$$Q_{L\uparrow} = Q_{L\downarrow} \cdot A_L + (1 - A_L) \cdot \sigma \cdot T_s \quad (2.2)$$

$$\sigma \approx 5.67 \times 10^{-8} \text{ J} \cdot \text{m}^{-2} \cdot \text{s}^{-1} \cdot \text{K}^{-4}$$

where $Q_{L\downarrow}$ contains both the reflected heat from the atmosphere and the emitted heat from the surface. The emitted heat radiation from the surface depends on the surface temperature (T_s), Almkvist (2020). According to Peterson & Ringström (1977), the heat radiation from the surface is typically higher than the radiation from the atmosphere ($Q_{L\uparrow} > Q_{L\downarrow}$), leading to a small energy loss for the surface in terms of longwave radiation. The small energy loss in terms of longwave heat radiation, means that the supplied energy to the surface, primarily depends on the amount of radiation from the sun, Q_S . The total radiation, Q_N , can be described as

$$Q_N = Q_S - Q_R + Q_{L\downarrow} - Q_{L\uparrow} \quad (2.3)$$

The energy balance does also include the heat exchange parameters Q_A , Q_{EC} , Q_{MF} , and Q_G , Q_H , which will be described in this paragraph. The heat from traffic, Q_A , is heat added to the road caused by the friction from wheels, and the heat from motors, Almkvist (2020). The parameters Q_{EC} and Q_{MF} , describe heat added or deducted to the surface from water undergoing a phase change. According to Almkvist (2020), there are four types of phase changes that need to be taken into consideration: condensation, evaporation, melting and freezing. If the water in the air is condensing, energy is added to the surface as latent heat, Almkvist (2020). During evaporation, heat energy is deducted instead. The heat from condensation and evaporation is described by the parameter Q_{EC} . Almkvist (2020) describes that when water on the surface freezes, it releases heat energy to the surface, and when

water is melting, energy is deducted from the surface to the water. The heat from freezing and melting is described by the parameter Q_{MF} .

The parameter Q_G describes the heat exchange between the ground below the surface and the surface itself, Peterson & Ringström (1977). Similarly, Q_H describes the heat exchange between the air layer above the surface and the surface, Peterson & Ringström (1977). According to Almkvist (2020), these two parameters are dependent on the heat conductivity of the material in the ground and the heat conductivity of the air layer above. The heat exchange between the air layer and surface is also dependent on the wind. If these two parameters add or deduct energy to the surface depends on whether the surface is under heating or cooling process, Peterson & Ringström (1977).

The cooling process is typically illustrated by night time, see figure 2.4. What characterizes the heat exchange during night time is the lack of radiation from the sun and sky Q_S , which is the most significant energy source, Peterson & Ringström (1977). The surface will then lose heat to the surrounding air, and the surface will cool off, as a result of $Q_{L\uparrow}$ being more significant than $Q_{L\downarrow}$. The heat loss will be compensated by added heat energy from the ground below the surface, with a positive Q_G , Peterson & Ringström (1977). The amount of energy added depends on the material properties in the ground. The air above the surface can, depending on its temperature, either add or deduct heat energy from the surface. If the air layer above the surface has a higher temperature than the surface itself, heat from the air will be conducted to the surface and vice versa. It is common that air colder than the surface is brought in by wind from the surrounding environment and cools down the surface. The cooling process is also affected by phase changes. If condensation occurs, trough dew or frost, energy will be released from water to the surface and therefore counteract the cooling process, Peterson & Ringström (1977).

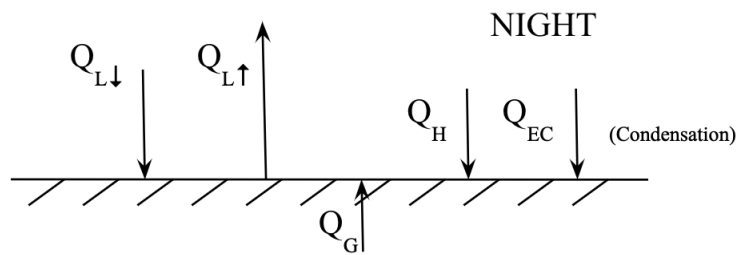


Figure 2.4: The figure illustrates the energy balance of the surface during a typical night. The authors' own illustration.

The heating process is typically illustrated by day time, see figure 2.5. During the day, unlike night, the dominating parameter is incoming radiation from sun and sky, Q_S , heating the surface. According to Peterson & Ringström (1977), the temperature of the surface becomes higher than the air layer above and the ground below. Excess heat is then conducted from the surface and stored in the ground, leading

to a negative flow of Q_G . The air layer above is also heated by the surface, through a negative Q_H . The heat in the air is transferred to the surrounding environment with the wind. The high temperature of the surface leads to water evaporating instead of condensation, which gives a small energy loss through a negative Q_{EC} . The energy loss from evaporation is not significant for the surface itself, but rather for the surrounding terrain.

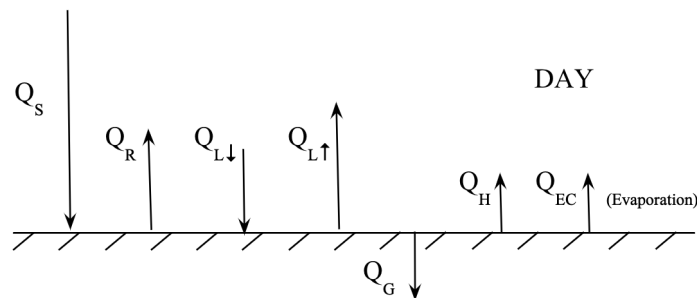


Figure 2.5: The figure illustrates the energy balance of the surface during a typical day. The author's own illustration.

2.2.2 Environmental factors affecting the energy balance

The environmental factors affecting the parameters in the energy balance are defined by Almkvist (2020) as sky view factor (SVF), traffic amount, meters above sea level, road heat conductivity (RHC), road surface temperature (T_s), air temperature (T_a), relative humidity, wind, precipitation, and cloud. One of these is, as seen, the road surface temperature, T_s , which is the factor that the model is set up to forecast. In this section, the environmental factors that affect the energy balance, aside from road surface temperature, are further described. These factors need to be taken into account in the climate model to forecast road surface temperature.

Some of the environmental factors are described as constant parameters in the climate model for each specific location. These constant parameters are SVF, meters above sea level, and traffic amount. The parameters regarding road construction and RHC are described as constant parameters for all of Sweden. The factors, air temperature, relative humidity, wind, precipitation, and cloudiness, will fluctuate during the day and are described as variables in the climate model. The information about these is collected from RWIS and SMHI.

According to Dirksen et al. (2019), the SVF describes how much of the sky that is exposed, and thereby the amount of direct sunlight that hits the surface, which affects the parameter Q_s in the energy balance. At a point where the SVF= 0, the entire sky is blocked from view by obstacles, and SVF= 1 represents an open sky with full exposure. The SVF is calculated based on the horizontal angles, which describe the distance and height of a object that hinders the direct sunlight. The horizontal angles are affected by vegetation, topography, and building in the surrounding environment. When the sun is lower than the horizontal angles, shadows

2. Theory

are created on the road. In other words, the horizontal angles describe how vegetation and other surrounding objects, create shadows on the road. An illustration of how horizontal angles hinder direct sunlight throughout the day depending on the position of the sun, can be seen in figure 2.6.

According to Almkvist (2020), in the climate model, the SVF is specified for 24 sectors, 15°C each, around each station. The SVF is set to a constant value calculated based on the horizontal angle of each sector, and represent the fraction of the visible sky of the sector. In the climate model for car-borne roads, the horizontal angles and the SVFs are collected from Google Maps via street view. The sectors that are of most importance when it comes to the SVF are the sectors representing the direction where sunrise and sunset occur. This is because of shadows on the road during sunrise or sunset delay the heating or cooling process. A well-timed heating or cooling process leads to more accurate road surface temperature forecasts throughout the day.

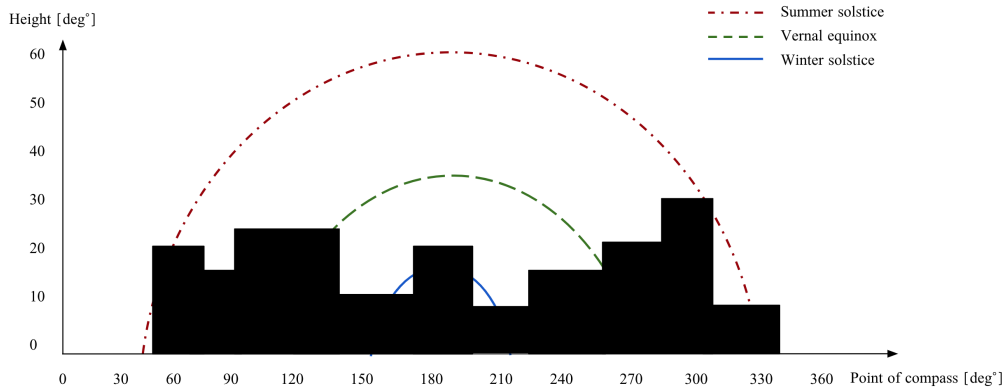


Figure 2.6: Illustration of solar position for vernal equinox, summer and winter solstices. The horizontal angles are illustrated by the boxes and represent objects that hinder direct sunlight. The authors' own illustration.

Heat is added from traffic through Q_A in the energy balance, caused by friction from wheels and heat from motors. Q_A is affected by the environmental factor traffic amount. If the amount of traffic is high, the heat added from traffic to the surface in the energy balance will also be high. In the climate model, there are two different ways of defining the amount of traffic. The first way is to set it to a default value of 15 W/m^2 added from traffic. This value is based on calculations from the open-source software model, called METRo, (Crevier & Delage, 2001, p. 2028). The second way is to specify the amount of traffic for each location, and thereby get a more realistic result. In the second case, the amount of traffic is based on a mean value collected from the Swedish Transport Administration. The mean value is called Årsmedel Dyngs Trafik (ÅDT), Trafikverket (2020), and describes the mean value of traffic passing a specific road segment during a day. In the climate model, the environmental factor traffic amount is set to a constant mean value for each location, based on its ÅDT. The mean value is then recalculated in the algorithm

to follow the rhythm of the traffic during a day. During workdays, the traffic load is higher during mornings and afternoons, and during weekends, the amount of traffic is evenly distributed during the day, Almkvist (2020).

The environmental factor meters above sea level affect the topography of the location. The topography of a road segment and the topography of the surrounding determines the topoclimate of the location. The topoclimate does, for example, steer the wind, affect the amount of shortwave radiation that reaches the ground, the air temperature, and cloudiness. The different topoclimates and how they affect the road climate are described in detail in section 2.1.3.

The heat exchange with the ground below the surface, Q_G , is affected by road construction. The heat transfer is affected by which materials the road is constructed with and how the materials are layered. In the climate model, the material layers, their thickness, and heat conductivity are set to constant values for all of Sweden through the parameters thickness of the asphalt and underlying layers, and RHC. The heat conductivity for typical materials used for road construction is shown in table 2.2. In the climate model, the standard layers are set by Klimator and are confidential.

The layer that affects heat transferring the most is the thickness and RHC of the top layer of asphalt. According to Almkvist (2020), the RHC of asphalt is mainly determined by how porous the asphalt is. If the asphalt is porous, the asphalt can contain air or water blisters, which transfers heat slower than the asphalt itself. Therefore, porous asphalt isolates heat better than compact asphalt resulting in a lower RHC, i.e., heat transferring slower, for porous asphalt. If the surface has a low RHC, less heat will be transferred to the underlying layers, and more heat will be left in the surface itself.

Table 2.2: Heat conductivity for materials that are normally used to construct roads.

Material	Heat conductivity [$WK^{-1}M^{-1}$]
Asphalt	0.80
Concrete	2.20
Deep soil	0.95
Crushed rocks	1.00

The fluctuating environmental factors affecting the incoming radiation, Q_S , are precipitation and cloudiness. Precipitation may result in snow and ice, affecting the albedo of the surface. Snow and ice primarily affect the shortwave albedo, A_S , while the longwave albedo, A_L , stays practically the same. In other words, when the surface is covered with snow or ice, shortwave radiation is reflected to a much greater extent, leading to less radiation from the sun and sky being absorbed by the surface, Almkvist (2020).

Furthermore, clouds affect both Q_S and $Q_{L\downarrow}$ and have a significant impact on the temperature difference between day and night. During the day, clouds prevent short-wave solar radiation from reaching the ground. The amount of radiation hindered by clouds depends on the cloudiness, which is measured in parts of eights. Since the radiation from the sun and sky is the most significant parameter affecting the road temperature, the road surface temperature becomes significantly lower on a cloudy day. At night, clouds hinder outgoing heat from the surface to enter the atmosphere. The heat is then reflected by the clouds and absorbed by the surface through $Q_{L\downarrow}$. This means that on a cloudy night, the cooling process is slowed down due to an increased $Q_{L\downarrow}$ and the road surface temperature becomes higher than when it is clear sky, Lindqvist et al. (1983). The air temperature during a clear day and night, in comparison to a cloudy day and night, is described and illustrated in section 2.1.1 and figure 2.1.

In the energy balance, heat is exchanged between the surface, and the air above the surface, through the parameter Q_H . This heat exchange is affected by two environmental factors. These are air temperature, T_a , and the wind. These two environmental factors will affect the air layer's temperature closest to the surface, which will affect Q_H . How wind affects the air temperature close to the surface is described in section 2.1.1, which in turn affects Q_H . If the temperature of the air layer above the surface is higher than the surface temperature, heat will be transferred from the air to the surface, and the surface temperature will rise. The opposite will happen if the air temperature is lower than the surface temperature, Peterson & Ringström (1977).

The relative humidity and the air temperature, T_a , together determine the dew/freezing point. As explained in Lindqvist et al. (1983), the dew/freezing point affects the formation of dew, fog, and frost and describes how much water the air can hold before condensation/sublimation or evaporation. This is described further in section 2.1.1. The dew/freezing point affects the parameter Q_{EC} in the energy balance. Another factor that affects the condensation/evaporation, i.e., Q_{EC} , is the wind since it transports air containing new masses of water vapor, which can be deposited. Thus hoarfrost layer created from sublimation is thinner when the wind is calm and thicker when the wind is stronger, Lindqvist et al. (1983).

Precipitation and wind affect the amount of water on the surface. Precipitation is water in various forms falling from the earth's atmosphere. The wind affects how much precipitation that stays on the surface since it can speed up the drainage and drying process. The amount of water affects the temperature of the surface through the parameter Q_{MF} . When the water is undergoing a phase change, i.e., freezing or melting, heat exchange between the water and the surface occurs. Usually, the effect of the phase change is that the road temperature is preserved during a period, as a result of the heat exchange. Almkvist (2020) explains that this means that if the surface is under a cooling process, a plateau is created around the water's freezing point for the road surface temperature until the phase change is done. The water's freezing point depends on the amount of salt on the surface, and usually, the freezing point is moved from 0°C to -8°C on a salted road.

2.2.3 The process of the climate model when creating road surface temperature forecasts

The climate model is a part of the RSI solution and aims to create a road surface temperature forecast with the help of the energy balance and environmental factors. The environmental factors SVF, traffic amount, the thickness of the asphalt and underlying layers, and RHC are set manually to constant values for each location. The variable parameters in the climate model need to be processed continuously and are collected from both sensors along the road, called RWIS, and SMHI forecasts. What separates the two data sources is that RWIS gives actual measured values from local points along the road, while SMHI gives forecast data. The variable inputs and their sources are listed in table 2.3. When processing the variable parameters, the climate model works in two steps. During the first step, analyzing, the variable weather parameters are analyzed in 8-0 hours before the forecast. During this step, the variable parameters are used to adjust the energy balance. In the second step, forecasting, the climate model uses the adjusted energy balance to create a road surface temperature forecast.

Table 2.3: The table shows the sources for the variable input parameters for the algorithm.

Parameter	RWIS (measured value)	SMHI (forecast)
Road surface temperature	X	
Air temperature	X	X
Cloud		X
Dew point	X	X
Wind	X	X
Precipitation	X	X

During the analyzing step, 8 hours before the forecast, weather data from RWIS is used in an iterating process to adjust the energy balance. The variable parameters that are available from RWIS are collected as measured data. The parameter cloud is collected from SMHI since it is not available from RWIS, see table 2.3. Since SMHI data is limited to forecasts and not measured values, the insecurity of cloudiness becomes higher than the other parameters.

In the first step, road surface temperature data from RWIS is used as a reference, and the other variable parameters are used as inputs. In the first iteration, the parameters are used directly, with their exact value from RWIS, to calculate the surface temperature in the energy balance. The first result from the energy balance is then compared to the measured surface temperature from RWIS. The parameter values in the climate model are then adjusted in an attempt to get the second calculated value closer to the measured surface temperature. This process is repeated, and parameters are adjusted until the calculated surface temperature from the energy balance is within the couple limit, set by Klimator, from the measured

value. The resulting adjustments of the energy balance and its parameters are valid 5 hours ahead, but with a decreasing effect. For example, if the longwave radiation is adjusted with 10% for the algorithm to reach the couple limit, it will be adjusted 10% and then fall off, down to 0% during the next 5 hours. The iterative process is illustrated in figure 2.7.

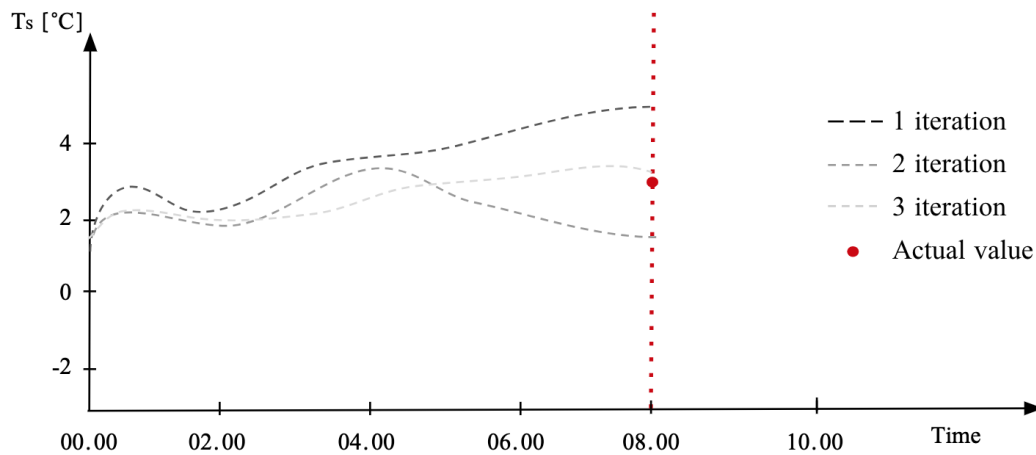


Figure 2.7: The figure is a rough illustration of the iterative process of the algorithm. The gray dashed line illustrates the iteration of the energy balance to calculate a road surface temperature. The vertical dotted red line marks the start of the forecast, and the bold red dot shows the actual value measured by RWIS. The authors' illustration.

The second step, forecasting, begins at the set start time for the forecast. During the second step, the modified energy balance is used to create a forecast from the start time and 18 hours ahead. When the forecast is created, no measured values from RWIS exist, only forecast data from SMHI is available. Since SMHI gives forecasts for local climate areas, it can be unreliable for the microclimate areas that are analyzed in the climate model. The data from RWIS, however, is measured values for the microclimate areas that are analyzed, and are therefore more reliable than the forecast data from SMHI. The unreliability of SMHI data is corrected by merging the measured values from RWIS that are available at the beginning of the forecast with the SMHI data. The values are relaxed together so that the values are closer to RWIS data at the beginning of the forecast, and closer to SMHI data as time passes. The merge of RWIS and SMHI data is illustrated in figure 2.8. The merged values are then used in the modified energy balance with the adjustments from step one, to calculate road surface temperature forecast.

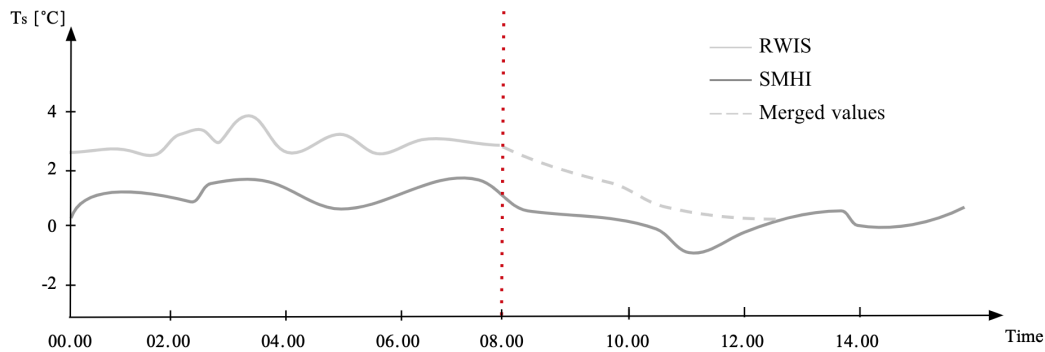


Figure 2.8: The figure is an illustration of how the measured value from RWIS at the start of the forecast, is relaxed together with the forecasts from SHMI. The red dotted line marked the start of the forecast. The authors' own illustration.

2.3 Research regarding differences between car-borne roads and bicycle paths

The current models for forecasting road surface temperature, RSI, and METRo, are developed for car-borne roads. In this section, the differences between car-borne roads and bicycle paths are presented. It is further described how the climate model is affected by these differences. This information will be used to modify and adapt the climate model to bicycle paths later on in the project. The differences presented in this section are the construction of the road, traffic amount, SVF, and sensors along the road. It should be noted that there might be other differences between bicycle paths and car-borne roads, which might not be defined in this thesis.

2.3.1 Construction of car-borne roads and bicycle paths

The construction of the road affects the heat exchange between the surface and the ground below the surface. The most critical factor affecting the RHC parameter is the properties of the top layer, asphalt. If the asphalt is porous, it might contain air- or water bubbles, which hinders heat from spreading in the material, resulting in lower heat conductivity for porous asphalt, i.e., heat transferring slower. Another factor affecting how fast heat is transported between the surface and the ground is the thickness of the material layers used to construct the road. The construction might differ between bicycle paths and car-borne roads as a result of different requirements and standards.

According to the Swedish transport administration, Trafikverket (2011), the regulations and requirements for car-borne roads regarding construction are based on traffic load, climate zone, and environment. Since the restrictions are based on many factors, the thickness of the asphalt and underlying layers seem to vary a great deal through Sweden. However, according to (Trafikverket, 2011, p. 8,13,21-26), require-

ments regarding the thickness and construction of the different layers are tougher for car-borne roads than for bicycle roads, as a result of bicycle paths being classified for lower loads. Observe that more specific regulations are added if the path is being maintained during the winter.

Regarding the type of asphalt, there are no apparent restrictions or standards regarding porosity and grain thickness, Trafikverket (2011). This means that the asphalt type could differ between car-borne roads and bicycle paths, although this is not stated in the restrictions. Below is a description of the different types of bicycle paths that dominate the Swedish cycle path network.

In Sweden, a couple of bicycle paths are dominating the path network. According to Hedström (2013), these are graveled paths, cycle zones, and separate bicycle paths. Cycle zones are the type of bicycle paths fully connected to car-borne roads and are commonly seen at 2+1 roads. Due to the placement in line with car-borne roads, the structure and construction are identical and follow the same regulations and restrictions as car-borne roads due to being built simultaneously. In some cases, a graveled path is preferable, but since they do not meet the requirements for winter road maintenance, they will not be further described in this report. The third option, often seen connected to cities, are the separate bicycle paths. Separate bicycle paths are constructed to ensure that winter road maintenance is possible. A difference between separate bicycle paths and car-borne roads are the priorities when constructing the roads. For example, according to Wågberg (2013), the need for flexibility is higher for separate bicycle paths, so that the paths can be able to handle movements in the ground. These movements in the bicycle paths are results of poor drainage and thin coating in comparison to the car-borne road. An example of car-borne roads is high-traffic rural roads, where abrasion resistance, deformation resistance, smoothness, friction, surface water capacity, and light reflection is prioritized instead, Wågberg (2013). Different priorities can affect the thickness of the asphalt and the type of asphalt used for bicycle paths compared to car-borne roads, affecting the parameters asphalt thickness and RHC in the climate model.

2.3.2 Local differences affecting the climate model

In this section, the local differences, such as traffic amount, SVF, and sensors available along the road, are presented. In the current climate model for car-borne roads, the amount of traffic is based on ÅDT gathered from the Swedish Transport Administration. The amount of traffic is then translated to heat added to the surface, caused by tires and motor. For bicycle paths, there are two significant differences regarding heat added from traffic. Firstly, the Swedish Transport Administration does not supply ÅDT for bicycle paths, meaning that it needs to be another method for estimating the traffic on bicycle paths. In this project, the bicycle paths examined were placed in Jönköping, where it was found that the local municipality had eight measuring points for passing bicycles reported by Gustafsson (2019). There is no guarantee for other municipalities measuring the number of bicycles, which means that this needs to be examined locally for every municipality if the information regarding the number of bicycles is needed. Secondly, since bicycles often have two

thinner wheels, instead of four tires, and operate without a motor, heat transferred to the surface by traffic should be considerably lower on bicycle paths compared to car-borne roads. According to Almkvist (2020), the current climate model is not constructed to translate the amount of traffic to heat added from bicycles, which needs to be taken into consideration when estimating heat from traffic on bicycle paths. The differences regarding the traffic amount will be taken into account by adjusting the traffic amount parameter in the climate model.

In the current climate model, SVF needs to be calculated for every station. To be able to calculate SVF, the horizontal angles are needed. Usually, the horizontal angles can be collected from street view in Google Maps for every 15 ° around the stations, resulting in 24 sectors around each station. The car-borne road network is highly covered by Google street view, but the coverage is low for bicycle paths. Due to the lack of street view, the horizontal angles for bicycle paths, in comparison to car-borne roads, need to be calculated manually.

Another local difference for bicycle paths and car-borne roads are the sensors along the road and the type of data they collect. Along car-borne roads in Sweden, there are approximately 775 RWIS, collecting local weather data. For bicycle paths, no structured weather station network exists. How a sensor network should be constructed for bicycle paths will not be discussed in this report.

In this project, Hede stations will be installed on bicycle paths and used to collect local weather data. Hede stations, in contrary to RWIS, do not collect data regarding wind speed or precipitation. This means that a climate model would need to use forecasts from SMHI for wind speed and precipitation when using Hede as a source for local weather data. Since locally measured data is more accurate for the road climate, using SMHI forecasts could lead to insecurities in the climate model. The different weather data measured for Hede stations and RWIS is summarized in table 2.4. The table only shows weather data that is relevant for the climate model when calculating road surface temperature.

Table 2.4: The table shows the different weather data that is measured for Hede stations and RWIS. The table only shows weather data that is used in the climate model to calculate surface temperature, and does not include other data.

Parameter	Hede	RWIS
Road surface temperature	X	X
Air temperature	X	X
Relative humidity	X	X
Wind		X
Precipitation		X

2.4 Evaluation tools

There are different ways to measure the accuracy of predictions. In this chapter, the three evaluating tools mean absolute error (MAE), root mean square error (RMSE), and confusion matrix will be presented and explained.

According to JJ (2020) MAE is characterized by describing the error without considering the direction of the error as a result of taking the absolute value of the calculated error. MAE is also designed not to consider the magnitude of the error. The error is, therefore, of equal weight. MAE is described by

$$\text{MAE} = \frac{1}{n} \sum_{j=1}^n |y_j - \hat{y}_j| \quad (2.4)$$

RMSE does, in contrary to MAE, consider the magnitude of the error, which is possible by applying quadratic scoring, JJ (2020). RMSE is described by

$$\text{RMSE} = \sqrt{\frac{1}{n} \sum_{j=1}^n (y_j - \hat{y}_j)^2} \quad (2.5)$$

Taking the size of the error into account is especially beneficial when large errors are undesirable. A confusion matrix shows how a classifier is confused when making predictions. Data School (2014) describes how a confusion matrix visualizes and summarizes the performance of a classification model by presenting a number of correct and incorrect predictions in a two by two matrix, a so-called, binary classifier. By defining the two classes positive and outcome, the four scenarios true positive, false positive, true negative, and false negative, can be described. Depending on what information that is of interest, different derivation rules can be combined and applied to the outcome from the binary classifier, Data School (2014). A confusion matrix does, therefore, provide both an understanding of what type of errors that occur as well as the number of errors. This breakdown is the advantage of the confusion matrix and overcomes the limitation of measuring accuracy alone. In figure 2.9, the definitions of the four scenarios, as well as the derivation rules used in this thesis, will be presented.

		Actual Values			
		Positive (0)	Negative (1)		
Predicted Values	Positive (1)	True Positive (TP)	False Positive (FP)	True Positive Rate (TPR): $TPR = \frac{\sum TP}{\sum \text{Positive}}$	False Positive Rate (FPR): $FPR = \frac{\sum FP}{\sum \text{Negative}}$
	Negative (0)	False Negative (FN)	True Negative (TN)	False Negative Rate (FNR): $FNR = \frac{\sum FN}{\sum \text{Positive}}$	True Negative Rate (TNR): $TNR = \frac{\sum TN}{\sum \text{Negative}}$
		Total population		Accuracy = $\frac{\sum TP + \sum TN}{\sum \text{Total Population}}$	

Figure 2.9: The scenarios of a binary confusion matrix and the rates that will be calculated in this project. Note that Σ Positive and Σ Negative is the summations of when the actual values are positive or negative.

3

Methodology

The project's methodology consists of two parts: installing sensors to obtain measured data and modifying the climate model for car-bone roads. The installation of stations included mounting and positioning of Hede stations on bicycle paths, described in section 3.1. The modification of the climate model was done through the four phases preparations, testing, evaluation, and validation. The method when modifying the climate model is described in section 3.2.

3.1 Installing Hede stations

The first part of the method was to install four Hede stations in Jönköping, to obtain measured weather data from bicycle paths. In this section, the process when installing the Hede stations is described. Firstly, the stations' positions were decided, and secondly, the stations were mounted and installed at decided locations. The stations were mounted on February 12 and 13.

3.1.1 Positioning of the Hede stations

The aim when positioning the stations was to create a variety of different types of microclimate. The aim was also to get coverage of the bicycle path network and to pinpoint places where the risk for slip is high. It is critical to create a geographical distribution and to cover several types of microclimate where slip can occur so that the climate model can be tested for a variate set of measured values. The four stations were placed within 3,5 km from each other, which covered both city and rural parts of Jönköping, see figure 3.1. The different types of microclimate covered by the stations will be explained below.

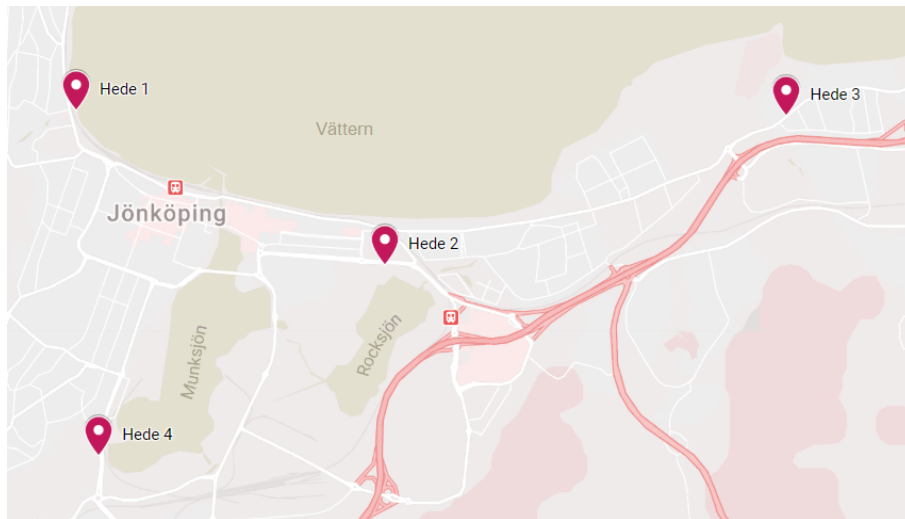


Figure 3.1: A map showing how the stations were placed in Jönköping.

The first station, Hede station 1, was placed at Västra strandpromenaden (57.789694N, 14.149926L), with the lake Vättern approximately 15 meters to the east. It is located at a flat and well-exposed grass area, which means that it has full sun and wind exposure. The station's western sector is urban, and in the eastern sector, the large water body of Vättern is placed. As a consequence of the water body not freezing during winter, the bicycle path is exposed to increased levels of moisture in the air. The increased level of moisture leads to a higher risk for black ice and hoarfrost formation, and this area is therefore seen as a critical point regarding slip. The location is visualized in figure 3.2. According to Holst (2020), the bicycle path at this location is constructed with the first layer of 150 mm reinforcement, the second layer of 150 mm gravel bearings, and at last 30 mm asphalt.



(a) A picture showing the first station's eastern sector with Vättern.



(b) A picture showing the bicycle path near Hede station 1.

Figure 3.2: Pictures showing the surrounding of Hede station 1.

The second station, Hede station 2, was placed at Odengatan (57.779084N, 14.189625L), connected to the centrally located park area, Knektaparken. The area surrounding the station is in a flat, open landscape with a green area on one side, and a car-borne road on the other side. Normally city centers are considered to be heat islands, but in this case, the sensor is located at a park cool island, where the lack of buildings nearby makes the area exposed to outgoing radiation and faster cooling at night. The location is visualized in figure 3.3. The information was given by Holst (2020) that the bicycle path is constructed with a first layer of 218 mm gravel bearings and a second layer of 32 mm asphalt.



(a) A picture showing the car-borne road near Hede station 2.



(b) A picture showing the park near Hede station 2.

Figure 3.3: Pictures showing the surrounding of Hede station 2.

The third station, Hede station 3, was placed at Huskvarnavägen (57.789319N, 14.241567L). The station is positioned in a rural area, which is typically cooler than city areas. Unlike the other stations, this station is placed on a local height, which means a relative difference in the surrounding topography. That the station is placed on a local height could lead to lower temperatures at this station. Furthermore, a land bank creates shades from Southeast that leads to a bigger horizon angle when the sun rises. This means that the road will be shadowed during the morning and day. A consequence of the road being shadowed during morning and day is lower temperature and increased risk for local slippery parties. The location is visualized in figure 3.4. The construction of the bicycle path at this location is unknown according to Holst (2020), since the municipality did not build it.



(a) A picture showing land banking with hoar, creating shadows on the bicycle path by Hede station 3. (b) A picture showing the bicycle path by Hede station 3.

Figure 3.4: Pictures showing the surrounding of Hede station 3.

The fourth station, Hede station 4, was placed at Jordbrovägen (57.766033N, 14.152839L), a rural area approximately located 40 meters from the open water body Munksjön. Similar to the first station, this station is exposed to higher moisture levels in the air, because of the water body. In the station's western sector, the risk for flooding is high due to forest and swamp areas. The vegetation in the western sector also creates shadows in the afternoon. The flooding and shadows can lead to ice formation on the surface of the bicycle path. According to Holst (2020), the bicycle path at this location is an old railway bank. The path is constructed with a basic rust bed, a reinforcement layer that varies in thickness, and a 100 mm gravel bearing layer. A few years ago, new asphalt was added with a depth of approximately 30-40mm.



(a) A showing the forest in station four's eastern sector. (b) A picture showing the forest and some flooding near Hede station 4.

Figure 3.5: Pictures showing the surrounding of Hede station 4.

3.1.2 The mounting process

When the positions of the stations were decided, the mounting process was performed in two steps. First, the Hede stations were assembled on metal poles, and second, the assembled stations were mounted onto lamp-posts along the bicycle paths in the four selected positions described in section 3.1.1.

Each Hede station was equipped with sensors that measured air temperature, relative humidity, and surface temperature, which were assembled onto a metal pole. The air temperature and relative humidity were measured by sensors mounted on top of the metal pole, 2 m above the ground. The height of 2 m above the surface is the conventional limit for microclimates, Peterson & Ringström (1977). The surface temperature was measured by a sensor at the end of a cable, which was drawn through the metal pole, allowing the surface temperature sensor to be close to the surface. The cable at the end of the metal pole was covered with a plastic PVC hose with 20 mm \varnothing . When each Hede station had been assembled on a metal pole, they were mounted following the process described below.

Each metal pole with Hede stations assembled was attached to the selected lamp-post with metal straps. A hole was then dug next to the lamp-post, with an approximate depth of 15 cm below the surface, to lead the cable measuring the surface temperature to the bicycle path surface, see figure 3.6.



(a) A picture of the hole that was dug out for the Hede station cable. (b) A picture showing the station in place and a semi-cover cable.

Figure 3.6: Pictures showing the hole and placement for the cable and its plastic cover.

The hole's depth was not calculated in advance but discovered on set to ensure that the cables and its surrounding cover would stay below the surface. The soil that was dug out was kept to be used as filling later on. A track with the depth of approximately 1 cm was milled in the asphalt with a cutter to create a space for the surface temperature sensor, see figure 3.7a. The sensor was placed in the track and

3. Methodology

covered with silicon, see figure 3.7b.



(a) A picture showing the milled track in the asphalt.



(b) A picture showing how the surface temperature sensor was covered.

Figure 3.7: Pictures showing how the surface temperature sensor was placed into the asphalt.

When the Hede station had been mounted the hole next to the lamp-post was covered using the stored soil. There were also small holes at the end of the metal pole that were covered with duct-tape to minimize the risk of water entering inside. Lastly, the supplied antenna was attached to the station to get a signal from the Hede station. A fully mounted station is seen in figure 3.8.



(a) A picture showing a fully mounted Hede station from afar.



(b) A close up of the ground by a fully mounted Hede station.

Figure 3.8: Pictures showing a fully mounted Hede station.

3.2 Modification of the climate model

In this section, the process and methods used when modifying the climate model, are described. The modification process was made in four phases, set up, testing, evaluation, and validation. The first phase included setting up an environment to be able to modify the climate model and to define which parameters were to be tested. A virtual environment in Docker was set up, and the collected data from the Hede stations were stored in a database in MySQL. Then knowledge from the theory was used to define the potential critical parameters which were going to be tested, as well as using the theory to define their default values. In the second phase, testing, each parameter was modified and tested individually on a test data set by running the climate model with each modification. The testing process included using theory and calculations to decide which values that were to be tested for each parameter. The testing phase was the most extensive one, since the same process needed to be repeated for each parameter that was tested. In the third phase, evaluation, the results from the second phase were analyzed through plots, and by using the mathematical formulas MAE and RMSE, see equation (2.4) and (2.5). During the evaluation phase, there was room to adjust the parameters further based on the results if needed. In the fourth phase, validation, the outcome from the evaluation phase led to a final modification, that was tested on a validation data set. The different steps will be described in detail in this section.

3.2.1 Setting up the testing environment and defining parameters

This section aims to describe the setup that was done to simulate and test modifications in the climate model. The climate model's algorithm is written in C# and is adapted to work in the operative system Linux. To be able to run the climate model without needing access to a Linux computer, a container with the algorithm software was built in Docker. A virtual Linux operative system with all software needed to run the climate model was created in the docker container. In the virtual environment in Docker, the software could be run and modified with so-called flags, without altering the original software.

Another part of the setup was to create a database in MySQL with data from the installed Hede stations and data from SMHI and connect it to the Docker container. In addition to the measured data from Hede, data from the three RWIS 648,651, and 653 in Jönköping was stored in the database as well. The purpose of storing data from RWIS was to run the modifications on the car-borne roads where the RWIS were placed, to see how the modifications applied on car-borne roads. The locations of both Hede stations and RWIS can be seen in figure 3.9. The reason for selecting the three RWIS in Jönköping was to have similar weather conditions at all stations.

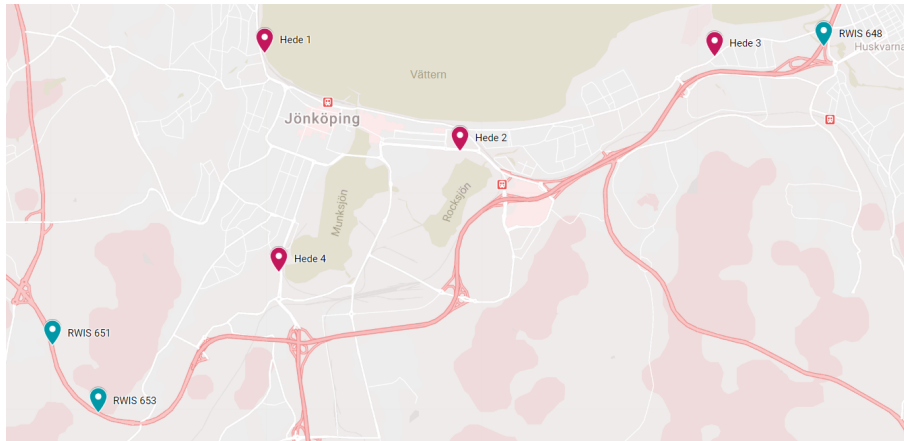


Figure 3.9: A map showing the locations of the Hede stations and RWIS measuring local weather data for this thesis

In MySQL, tables were created with the atmospheric data from SMHI, road station data with measured values from Hede and RWIS, and segment station data with local data, such as position, meters above sea level, and amount of traffic. In addition to segment station data, there were tables with local shading data used to calculate SVF. The atmospheric data contained weather forecasts for the local climate in Jönköping, such as cloud, wind, air temperature, and precipitation, from SMHI for every hour between February 27 and March 27. The road station data contained measured values from RWIS and Hede stations in Jönköping between February 27 and March 27. The local parameters, such as SVF and amount of traffic, could be altered via the MySQL database. These parameters were stored in segment station data and shading data.

After setting up the software and database, the parameters and their default values were defined for testing. Based on the theory about differences between bicycle paths and car-borne roads, described in section 2.3, it was decided to test the parameters SVF, traffic amount, the thickness of the asphalt and the underlying layers, and RHC. For SVF, the default value was set to 1, which corresponds to open sky and thereby full exposure, meaning no shadows on the road surface. The default value for traffic amount was taken from measurements performed by Crevier & Delage (2001) and was set to $15W/m^2$. The asphalt thickness and underlying layers were set to the thickness used by Klimator in their climate model. The exact asphalt thickness is, therefore, confidential. The road heat conductivity was set to 0.8, which is standard asphalt in Canada according to Crevier & Delage (2001) and represents a type of asphalt that is neither porous nor compact. The default RHC is referred to as RHC standard in this thesis.

After defining the parameters that were set up for modification and testing, a test data set was defined. Measured data from both Hede and RWIS was analyzed to get a varied data set with different weather situations. It was decided to use two different periods, February 27-29 and March 7-9, to get a more considerable weather variation. When analyzing errors in the evaluation phase, these two periods were

concatenated to one vector and treated as one continuous data stream. The last step of the preparations was to run the climate model with default values for each parameter on the test data set. The purpose of this step was to compare the forecasts with default values, with the forecasts made with each parameter modified. The parameters were modified one at a time, meaning that when one parameter was tested, all other parameters were set to their default values.

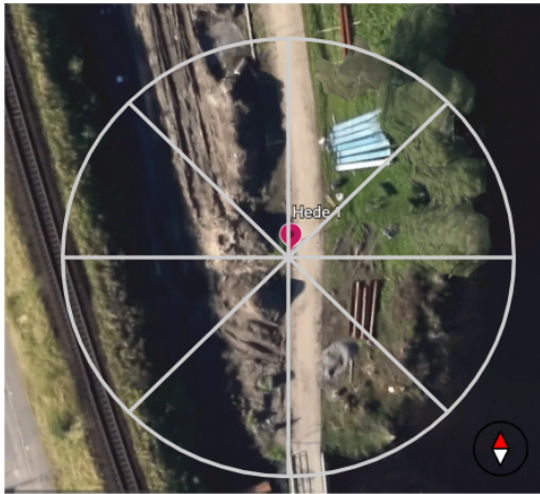
3.2.2 Testing SVF

The first parameter that was tested in the testing phase was the SVF parameter. The SVF parameter was tested by calculating the specific SVF for each station, with horizontal angles. The modifications were done by storing the modified SVF values in the MySQL database, in the table with shading data, and applying it to the climate model by using the flag `/Solar:true` Docker. The calculation for the second modification is described below.

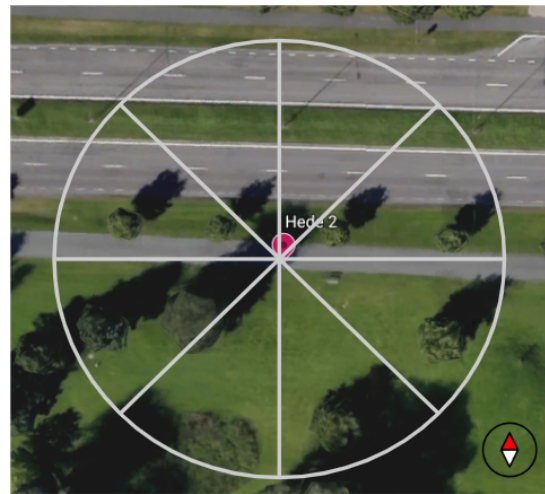
For the second modification, the SVFs were needed to be calculated for both RWIS and Hede stations. For RWIS, the SVFs were calculated by obtaining the horizontal angles from Google Maps street view. The horizontal angles for stations 648, 651 and 653, were collected for every 15 deg around each station, resulting in 24 sectors. The horizontal angles were then stored in the table with shading data in the MySQL database, making it possible to calculate SVFs for the stations in MySQL.

The car-borne road network is highly covered by Google street view, but for bicycle paths, the coverage is low. Due to the lack of street view for bicycle paths, the horizontal angle needed to be calculated manually. The horizontal angle was, therefore, simplified and was calculated for every 45 deg around the stations, instead of every 15 deg, which results in eight sectors (N, NE, E, SE, S, SW, W, NW) around each station. The precision was changed to eight sectors to still fit the sun's path, and include as much critical information as possible. For example, if only four sectors would have been used (N, E, S, W), the impact of sunrise and sunset would be excluded.

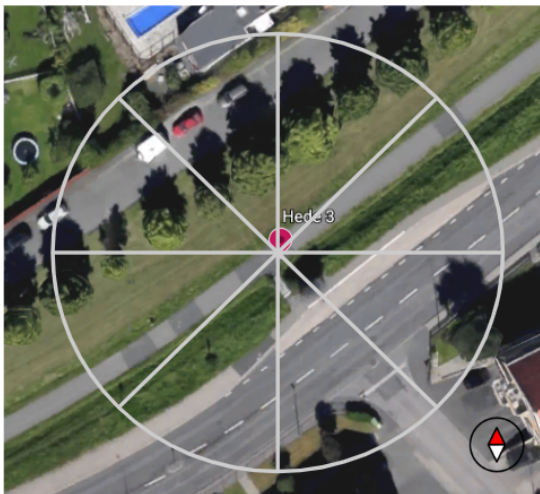
The method for calculating the horizontal angles followed the same pattern for all Hede stations. Firstly, each station was found using Google Earth to get a picture and overview of the surrounding from above. The surrounding of each station was then divided into eight sectors of 45 deg, starting at North. The sectors around the stations are illustrated in figure 3.10 below.



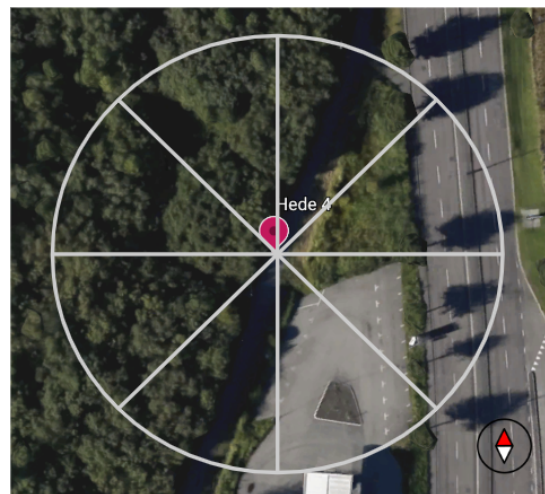
(a) A picture of Hede station 1 and its surrounding from above. The lines differentiates the eight sectors used when calculating horizontal angles. Observe the railway bank creating shadows in the western sectors.



(b) A picture of Hede station 2 and its surrounding from above. The lines differentiates the eight sectors used when calculating horizontal angles.



(c) A picture of Hede station 3 and its surrounding from above. The lines differentiates the eight sectors used when calculating horizontal angles.



(d) A picture of Hede station 4 and its surrounding from above. The lines differentiates the eight sectors used when calculating horizontal angles. Note the forest in the western sector that created shadows on the bicycle path were the station is placed.

Figure 3.10: The figures shows how the sectors used when calculating horizontal angles are divided around the Hede stations. The sectors are illustrated with sectioned light gray circles. The orientations of the pictures are noted with compasses in the lower right corners.

The horizontal angle of every sector around a station was calculated by finding the distance and height of significant objects in the sector in Google Earth. When height and distance from the station were obtained, the horizontal angle could be calculated for each object through equation

$$HA = \tan^{-1} \frac{h}{d} \quad (3.1)$$

h = height of object, d = distance to object from station

by using the trigonometric function tangent. How tangent was used to obtain the horizontal angle is illustrated in figure 3.11. If there were more than one significant object in one sector, the horizontal angle was calculated for all significant objects. The object with the largest horizontal angle was then selected as the final horizontal angle for the sector.

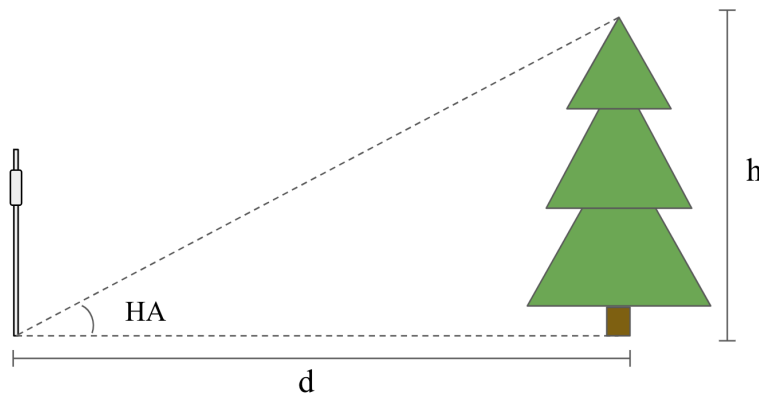


Figure 3.11: The figure illustrates how the horizontal angles were calculated with tangent for the different objects using their height and distance to the stations. In the figure HA stands for horizontal angle, d stands for distance between station and object, and h stands for height of the object.

When all horizontal angles for all Hede stations had been calculated, the angles were stored in the table with shading data in the MySQL database. The SVF for each sector was calculated from a 2D perspective through the equation

$$SVF_{2D} = \cos(HA) \quad (3.2)$$

for the Hede stations. The average SVF for each station, both Hede and RWIS, was calculated to get an overview of how shaded the surfaces around the stations were. The average SVFs, for both Hede and RWIS, can be seen in table 3.1. After storing the calculated values for SVF in MySQL, the climate model was run in Docker for every hour on the test data set (February 27-29 and March 7-9).

Table 3.1: The average SVF values for each station.

Station	SVF
Hede 1	0.74
Hede 2	0.71
Hede 3	0.63
Hede 4	0.36
RWIS 648	0.79
RWIS 651	0.52
RWIS 653	0.59

3.2.3 Testing traffic amount

The traffic amount parameter was the second parameter tested in the testing phase. Two different values were tested. The first modification was to set traffic amount to 0, representing no traffic, for all stations. The second modification was to use ÅDT for RWIS and to estimate the traffic amount for Hede stations. The modifications were done by storing the modified traffic amount values in the MySQL database, in the table with segment station data, and applied to the climate model by using the flag `/Traffic:true` in Docker. For the first modification, traffic was set to 0 for all stations in MySQL, and the climate model was then run with `/Traffic:true` for every hour on the test data set (February 27-29 and March 7-9). The process of estimating the ÅDT for Hede stations for the second modification is described below.

For the second modification, the specific traffic amount for each station needed to be stored in MySQL. For RWIS 648, 651, and 653, the traffic amount in MySQL was set to the ÅDT from the Swedish Transport Administration. For Hede stations, there was no data from the Swedish Transport Administration, and the heat added from traffic could not be directly translated from the amount of traffic. Instead, the amount of traffic was estimated using data from Gustafsson (2019). Then the amount of traffic for bicycle paths was adapted to translate the number of bicycles to a number of cars.

To estimate an ÅDT for the Hede stations, data providing an approximate number of passing bicycles at the stations where required. In Jönköping, eight bicycle counters count the number of bicycles passing in between April and October, Gustafsson (2019). The fourth station, Hede 4, was placed next to one of the eight bicycle counters located by Munksjögatan. Due to a lack of data at the remaining three Hede stations, the decision was made to calculate a ÅDT for Hede station four and assuming the same amount of passing bicycles for all stations. According to Gustafsson (2019), 300.000 bikes passed by Munksjögatan in between April and October. Through discussions with Klimator, the assumption was made that the traffic on bicycle paths decrease by 30% during the remaining five months of the year, the mean value of bicycles passing the station was estimated to 1000 a day. Since traffic in the algorithm was adapted for cars, the number of bicycles could not be directly stored and translated as the amount of traffic in the climate model.

It needed to be adjusted to represent the heat added from bicycles. There was no information regarding how much heat that is transferred from a bicycle to the surface. Therefore, the adjustment could not be based on calculations. Instead, the adjustment was made by discussing with Klimator and assuming that the heat from one bicycle was $\frac{1}{10}$ of the heat added from one car. The estimation and adjustment resulted in the amount of traffic being set to 100 passing cars a day for all Hede stations in MySQL. The resulting Traffic amount for the second modification, for both Hede and RWIS, can be seen in table 3.2. After setting the traffic to the specific ÅDT values for each station, the climate model was run with `/Traffic:true` for every hour on the test data set (February 27-29 and March 7-9).

Table 3.2: The estimated ÅDT for Hede stations and actual ÅDT for RWIS, used in second modification for traffic amount.

Station	ÅDT
Hede 1	100
Hede 2	100
Hede 3	100
Hede 4	100
RWIS 648	10200
RWIS 651	13140
RWIS 653	13140

3.2.4 Testing Asphalt and underlying layer thickness

The third parameter tested was the thickness of the asphalt and underlying layers. As described in section 2.3.1, bicycle paths are typically classified for lower loads in comparison to car-borne roads, which is why the thickness of the asphalt and underlying layers were modified. The thickness of the asphalt and underlying layers were modified with information from Jönköping municipality as background, obtained from Holst (2020) when positioning the stations. As seen in section 3.1.1, the actual thickness of the asphalt on the bicycle paths, where the Hede stations have been placed, was around 0.03 m. The underlying layer was 0.3 m crushed rocks. The parameters were modified by using the flags `/asphaltThickness:0.03` and `/crushedRockThickness:0.3` in Docker. As mentioned in section 2.2.2, the thickness of the asphalt and the underlying layers are set to a constant values for all of Sweden. Therefore, the parameters were set to the same values for all stations, both Hede and RWIS, when testing the thickness of the asphalt and the underlying layers, in contrast to SVF and traffic which were set individually for each stations. The climate model was run with these values for every hour on the test data set (February 27-29 and March 7-9).

3.2.5 Testing RHC

The fourth parameter tested in the testing phase was the RHC of the surface. From section 2.3.1, it can be seen that there are no apparent restrictions or standards regarding the asphalt type used when construction car-borne roads or bicycle paths.

This means that the porosity and thereby the road heat conductivity of the asphalt on the surface could differ between car and bicycle paths. Since the type of asphalt used for bicycle paths is not clear, the RHC parameter was tested with the four values RHC low, RHC standard, RHC medium-high, and RHC high, representing different types of asphalt. The low value represented porous asphalt, the medium-high, and the high value represented compact asphalt, with the highest value resembling concrete. The standard, which was the default value, represented standard asphalt according to Metro in Canada and was a value in between the low and medium-high RHC. As mentioned in section 2.2.2, the parameter RHC is set to a constant value for all of Sweden. Therefore, the RHC was set to the same value for all stations, both Hede and RWIS, when testing the RHC parameter, in contrast to SVF and traffic which were set individually for each stations. The modifications were done and applied to the climate model by using the flag `/heatCond` in Docker. The climate model was run for every hour test data set (February 27-29 and March 7-9), with the flag `/heatCond` for each RHC value tested.

3.2.6 Evaluating the testing phase and validating

When the climate model was run for every parameter individually, on the test data set, the resulting forecasts from the climate model were compiled in CSV files. The forecasts from the climate model were then compared against the measured data from Hede and RWIS. Each parameter was evaluated individually by plotting the forecasts against the measured values, and by calculating errors to measure the accuracy of the forecasts in Matlab. The two metrics that were used for measuring accuracy were MAE, and RMSE, described in section 2.4. When calculating errors, the two different periods in the test data set, February 27-29 and March 7-9, were concatenated to one vector and treated as one continuous data stream. A main script and functions were created in Matlab to extract forecasts, plot, and calculating errors.

Before the forecasts could be evaluated, the forecasts needed to be extracted from CSV files compiled by the climate model. There was one CSV file for every hour that the climate model had been run, containing 0-18 hour forecasts for every station. Firstly, the CSV files were sorted into folders based on parameters and changed value. This resulted in the one folder for default, one folder for SVF, two folders for traffic amount, two folders for asphalt thickness, and three folders for RHC. The forecasts were extracted from the CSV files by using a function called `load_forecast.m` created in Matlab, see Appendix A. The function was used in the main script to extract the 1-,4-, and 8-hour forecasts from all the folders with outputs from the test phase. The parameters SVF, traffic amount, asphalt thickness, and RHC were analyzed individually by plotting and measuring accuracy for all their values for 1-,4-, and 8-hour forecasts against the measured values from Hede and RWIS. The measured values were imported in the main script by using `load` in Matlab.

To visualize the results from the testing phase and to detect deviations, each parameter with its different values was plotted against the measured values from Hede and RWIS. Every station was plotted individually for the two different time spans

27-29 February and 7-9 March separately. Each plot showed the 1-,4- or 8-hour forecasts for one parameter with different values, against the measured value for the same station. When plotting SVF, it appeared that the calculated SVF for Hede deviated from both the default forecast, where full sun exposure was used and the measured values. The deviations were of the highest significance for Hede 4, where a clear temperature dip occurred in the middle of the day where the temperature should increase, see figure 3.12.

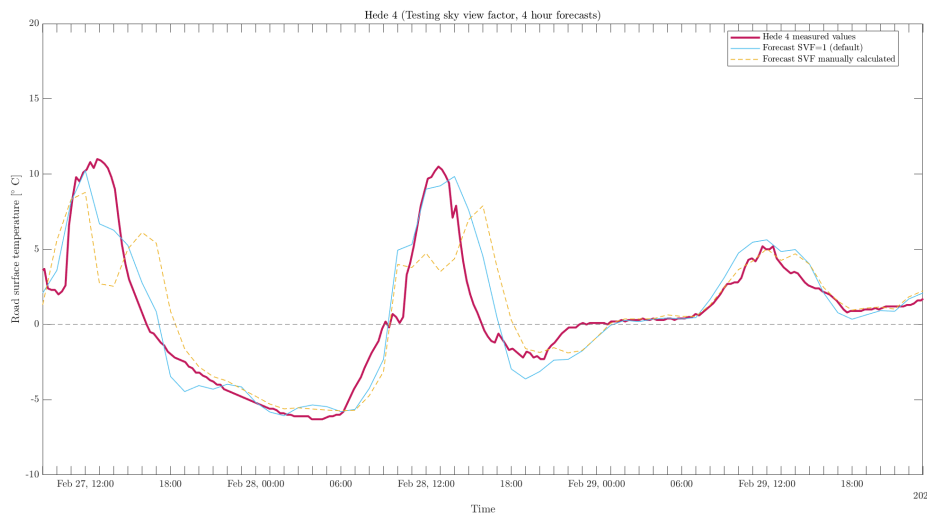


Figure 3.12: A plot showing the forecasts for surface temperature made with modifications on SVF for Hede 4. The plot illustrates the dip that occurs in the middle of the day with SVF manually calculated.

The deviations indicated that the horizon angles for sector five, which corresponds to $180\text{-}225^\circ$ and midday, were inaccurate. As mentioned in 3.2.2, SVF was calculated manually based on eight sectors instead of 24. This simplification of sectors was made to cover the critical hours of sunrise and sunset, which was thought to be detailed enough. When analyzing the sectors where the deviations occurred for Hede station 4, it was found that the variation in sun exposure was significant in sector five. It was decided to divide sector five into three smaller sectors and re-calculate the horizon angle for these. In figure 3.13 below, the sectors, when calculating the refined SVF is illustrated. For Hede station 1, there were some differences between the pictures from Google Earth and reality. Therefore the SVF for Hede station 1 was also slightly refined to fit reality better. The refined SVF values for Hede stations 1 and 4, seen in table 3.3, were re-entered into the database via MySQL, and the climate model was re-run with the refined values on the test data set. The resulting forecast was then compared against measured values by plotting and calculating errors.

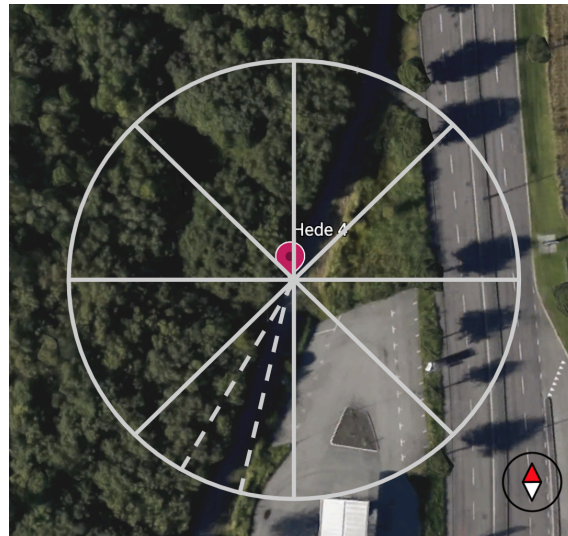


Figure 3.13: The figure illustrated the sections around Hede 4 after refinement. The stretched lines illustrates the sections added during refinement.

Table 3.3: The average SVFs for manually calculated SVF for all Hede and the manually calculated and refined SVF for Hede station 1 and 4.

Station	SVF manually calculated	SVF manually calculated and refined
Hede 1	0.74	0.79
Hede 2	0.71	-
Hede 3	0.63	-
Hede 4	0.36	0.44

After plotting, the errors were calculated, for every parameter value tested, through a function in Matlab. Since the forecasts were made for every whole hour and Hede and RWIS collected data for every 15 and 10 minutes respectively, the function first collected the measured values nearest every whole hour in time, using the Matlab function `retime`. The function then calculated the errors between a forecast and the measured values for every station, using the metrics MAE and RMSE described in section 2.4. The errors were also calculated for all Hede and all RWIS. The errors were calculated for 1-,4- and 8-hour forecasts. However, the most significant forecasts were the 4-hour forecasts, since the contractors maintaining the roads and paths need approximately four hours to act according to Gustavsson (2020). The MAE and RMSE from the 4-hour forecasts were compiled into two tables, for each parameter, one for Hede and one for RWIS. In the tables, the smallest error was highlighted for each station, all Hede combined, and all RWIS combined. Although the errors were calculated and compiled in tables for both Hede and RWIS, only Hede was used during the evaluation phase, see tables 3.4-3.7. RWIS were analyzed

later on in the process to pose as reference for recommendations regarding bicycle paths. In tables 3.4-3.7, the forecasts used when calculating the errors were 4-hour forecasts made on the whole test data set (February 27-29 and March 7-9). In the tables the smallest error for each station is highlighted.

Table 3.4: The table presents the MAE and RMSE for the forecasts where the SVF parameter was modified, around the Hede stations.

Station	MAE Surface temperature [°C]		RMSE Surface temperature [°C]	
	SVF manually calculated and refined	SVF=1 (default)	SVF manually calculated and refined	SVF=1 (default)
	Hede 1	0,927	0,898	1,264
Hede 2	0,931	0,989	1,379	1,443
Hede 3	0,891	1,003	1,168	1,351
Hede 4	1,001	0,955	1,446	1,358
All Hede	0,938	0,961	1,318	1,342

Table 3.5: The table presents the MAE and RMSE for the forecasts where the traffic amount parameter was modified, around the Hede stations.

Station	MAE Surface temperature [°C]			RMSE Surface temperature [°C]		
	Traffic 0	Traffic 15 W/m ² (default)	Traffic ÅDT	Traffic 0	Traffic 15 W/m ² (default)	Traffic ÅDT
	Hede 1	0,918	0,898	0,911	1,207	1,207
Hede 2	0,979	0,989	0,985	1,435	1,443	1,441
Hede 3	1,012	1,003	1,021	1,356	1,351	1,365
Hede 4	0,952	0,955	0,951	1,344	1,358	1,343
All Hede	0,965	0,961	0,967	1,339	1,342	1,341

3. Methodology

Table 3.6: The table presents the MAE and RMSE for the forecasts where the asphalt thickness parameter was modified, around the Hede stations.

Station	MAE			RMSE		
	Surface temperature [°C]			Surface temperature [°C]		
	Asphalt 3 cm Crushed 30 cm	Asphalt 7 cm Crushed 80 cm	Asphalt Klimator (default)	Asphalt 3 cm Crushed 30 cm	Asphalt 7 cm Crushed 80 cm	Asphalt Klimator (default)
Hede 1	0,903	0,909	0,898	1,213	1,223	1,207
Hede 2	1,019	1,003	0,989	1,497	1,461	1,443
Hede 3	1,045	1,012	1,003	1,410	1,361	1,351
Hede 4	0,972	0,965	0,955	1,391	1,372	1,358
All Hede	0,985	0,972	0,961	1,381	1,357	1,342

Table 3.7: The table presents the MAE and RMSE for the forecasts where the RHC parameter was modified, around the Hede stations.

Station	MAE				RMSE			
	Surface temperature [°C]				Surface temperature [°C]			
	RHC low	RHC stand (def)	RHC med	RHC high	RHC low	RHC stand (def)	RHC med	RHC high
Hede 1	0,874	0,898	0,968	1,030	1,215	1,207	1,309	1,407
Hede 2	1,120	0,989	0,965	0,940	1,659	1,443	1,374	1,343
Hede 3	1,175	1,003	0,929	0,886	1,643	1,351	1,234	1,174
Hede 4	1,022	0,955	0,957	0,985	1,450	1,358	1,370	1,440
All Hede	1,048	0,961	0,955	0,960	1,503	1,342	1,323	1,345

The tables were analyzed to select which values the different parameters of SVF, traffic amount, asphalt thickness, and RHC, should have in the validation phase. In the tables, the errors for all stations were displayed individually to display the distribution between the stations. However, the resulting error for all Hede was the one with the highest significance since these errors represent a higher variation in microclimate. As seen in tables 3.4, 3.6, and 3.7, the values with the smallest errors for all Hede combined were RHC medium-high, SVF manually calculated and refined, and Asphalt Klimator, which was the default value for asphalt. If both MAE and RMSE agreed, the value with the smallest error for all Hede was selected for validation. If the two calculated errors did not agree, as for traffic amount in 3.5, the results from the 8-hour forecasts were weighed in, as the errors in 8-hours forecasts are more pronounced. As seen in table 3.8, the value with the smallest errors for traffic was $15W/m^2$, which was the default value.

Table 3.8: The table presents the MAE and RMSE for the forecasts where the traffic amount parameter was modified, around the Hede stations. The forecasts used when calculating the errors were 8-hour forecasts made on the whole test data set (February 27-29 and March 7-9). In the table the smallest errors for each station are highlighted.

Station	MAE Surface temperature [°C]			RMSE Surface temperature [°C]		
	Traffic 0	Traffic 15 W/m^2 (default)	Traffic ÅDT	Traffic 0	Traffic 15 W/m^2 (default)	Traffic ÅDT
Hede 1	1,241	1,221	1,232	1,892	1,864	1,886
Hede 2	1,144	1,125	1,145	1,535	1,519	1,534
Hede 3	1,134	1,091	1,134	1,422	1,391	1,430
Hede 4	1,220	1,214	1,222	1,762	1,672	1,760
All Hede	1,185	1,163	1,183	1,663	1,621	1,662

When the values were selected, the validation phase was started. In the validation phase, the climate model was run two times, once with default values, and once with the values selected in the evaluation phase. I.e., the parameters were not modified individually, but all together. In the validation phase, the climate model was run every hour on a validation data set. The validation data set was set to be 27 February-27 March. When the climate model had been run with both default and modified values on the validation data set, the resulting forecasts were sorted, extracted, plotted, and accuracy was calculated in Matlab, following the same method as in the evaluation phase.

After following the same method as in the evaluation phase, plots, MAE, and RMSE were obtained for both default and modified forecasts on the whole validation data set. It was decided to add additional metrics and methods that isolated scenarios that were of higher significance when considering winter road maintenance and slip to give thorough discussion and recommendations. The first new metric was to calculate MAE and RMSE for temperatures close to zero since these are the most critical temperatures regarding slip. This was done by isolating data for both forecasts and measured values for the temperature span 5 to -5°C , and calculate MAE and RMSE for these data sets. The temperature was selected to balance the weigh-off between getting as close to zero as possible, without losing to many data points. The temperature interval was then discussed with the company which used the same interval.

The other method was to obtain a confusion matrix that was constructed to spot how often the forecast predicted positive and negative temperatures correctly. The confusion matrix was calculated based on the method presented in section 2.4. For the confusion matrices in this thesis, positive was set to be *temperatures above zero*. In this case, false positive meant that the forecast predicts temperatures above zero

when the actual temperature is below zero, which can result in a missed slip hazard. Therefore false positive gives a fatal error and is essential to detect. The forecasts were interpolated using spline interpolation with the Matlab function `retime`, to calculate the confusion matrices and match the amount of measured data obtained from Hede and RWIS. The two new metrics were calculated retroactively for the forecast obtained during the testing phase as well. This was done with the purpose of adding value and lay the ground for a thorough evaluation of the testing phase as well. When the two new metrics were calculated, the results from the evaluation phase and the validation phase were ready to be analyzed.

4

Results

In this chapter the results from the research regarding differences between car-borne roads and bicycle paths. Furthermore, the results from the test phase and validation phase will be presented, either as plots or as tables, and follows the same chronological order as in the method. Observe that results both from the Hede stations on bicycle paths, and from the RWIS on car-borne roads, will be presented in this chapter to enable comparative discussion. The results presented, will be further discussed in the following chapter Discussion 5.

4.1 Differences between car-borne roads and bicycle paths

Four differences between car-borne roads and bicycle paths were found throughout the research conducted in the beginning of the project and will be summarized in this section. The detailed information and sources from the research regarding differences between car-borne roads and bicycle paths, can be found in section 2.3.

Firstly, it was found that there are differences regarding the construction of the road and the thickness of the underlying layers. Although, the Swedish transport administration did not specify the thickness of the roads or bicycle paths, it was found that bicycle paths can be constructed to handle a lower load than car-borne roads. That bicycle paths are constructed to carry lower loads means that the asphalt and the underlying layer can be thinner than for car-borne roads. It was also found that the priority when constructing bicycle paths were to obtain flexibility, which might lead to using different asphalt thickness and asphalt material when constructing bicycle paths. Note that the Swedish transport administration carry out regulations and restriction, but the actual construction of the roads and bicycle paths are decided by the contractors.

Secondly, it was found that there are differences regarding the amount of traffic and how the information about the amount of traffic could be found. For car-borne roads the amount of traffic could be based on from the Swedish transport administration. The Swedish transport administration caters data for all of Sweden's car-borne roads network, but not for bicycle paths. For bicycle paths, data regarding the amount of traffic was found through the local municipality, Jönköping. Regarding bicycle paths

there were fewer locations that measured the amount of traffic, and in addition, the amount of bicycles could not be directly translated to the amount of cars in the climate model. This led to an estimation made in the method, leading to the results presented in table 4.1.

Table 4.1: The estimated ÅDT for Hede stations and actual ÅDT for RWIS, used in second modification for traffic amount.

Station	ÅDT
Hede 1	100
Hede 2	100
Hede 3	100
Hede 4	100
RWIS 648	10200
RWIS 651	13140
RWIS 653	13140

Thirdly, it was found that there are differences regarding the possibility to calculate SVF. Street view in Google Maps is used when calculating SVF for car-borne roads, and the calculations are therefore made through algorithms based on the surrounding environment. Google street view is well developed for car-borne roads compared to how little information that can be found for bicycle-paths in Google Maps. The lack of street view information means that the SVF was needed to be calculated manually for bicycle paths.

Lastly, it was found out that there are differences regarding measured data along car-borne roads and bicycle paths. For car-borne roads there is a structured network with RWIS along the roads throughout all of Sweden, but for bicycle paths there is no such network. In this project, four Hede stations were installed along the bicycle paths in Jönköping. A difference between Hede stations and RWIS is what weather data that is collected. The differences regarding weather data is summarized in table 4.2.

Table 4.2: The table shows the different weather data that is measured for Hede stations and RWIS. The table only shows weather data that is used in the climate model to calculate surface temperature, and does not include other data.

Parameter	Hede	RWIS
Road surface temperature	X	X
Air temperature	X	X
Relative humidity	X	X
Wind		X
Precipitation		X

4.2 Plots from the testing phase

In this section, the measured values from all Hede and RWIS, and selected results from the testing phase are presented in plots. The objective with visualizing the results in this format is to create an understanding of how a temperature forecast may look. In this section, the plots will only be presented for Hede 1 and RWIS 653 for traffic amount, asphalt thickness and RHC. The reason for presenting one Hede and one RWIS is that all Hede and all RWIS follow similar patterns although they differ in temperature magnitude. However, regarding SVF, all Hede stations will be presented since the results follow different pattern depending on the manual calculations for SVF. For RWIS, only one sensor will be presented. The motive for selecting Hede 1 and RWIS 653 when presenting traffic, asphalt thickness and RHC, is that the difference in temperature is greatest between these two sensors. Furthermore, the measured values from all Hede stations and RWIS will be presented so that the differences in microclimate are visualized in figure 4.1.

Observe that the plots below, in figures 4.2-4.12, show measured values and forecasts made on the time span February 27-29, which represent the first part of the test period. All plots show measured values and 4-hour forecasts where the parameters have been modified.

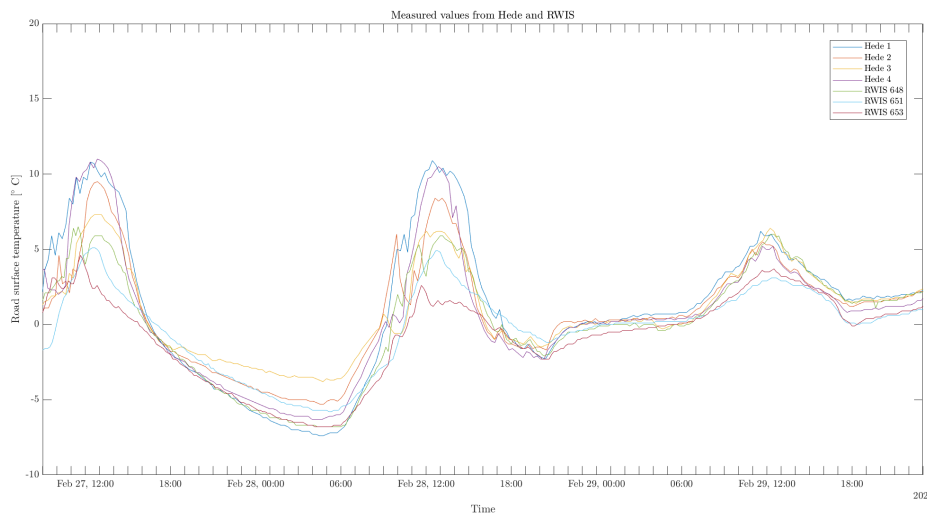


Figure 4.1: Measured values from all Hede stations and RWIS.

4. Results

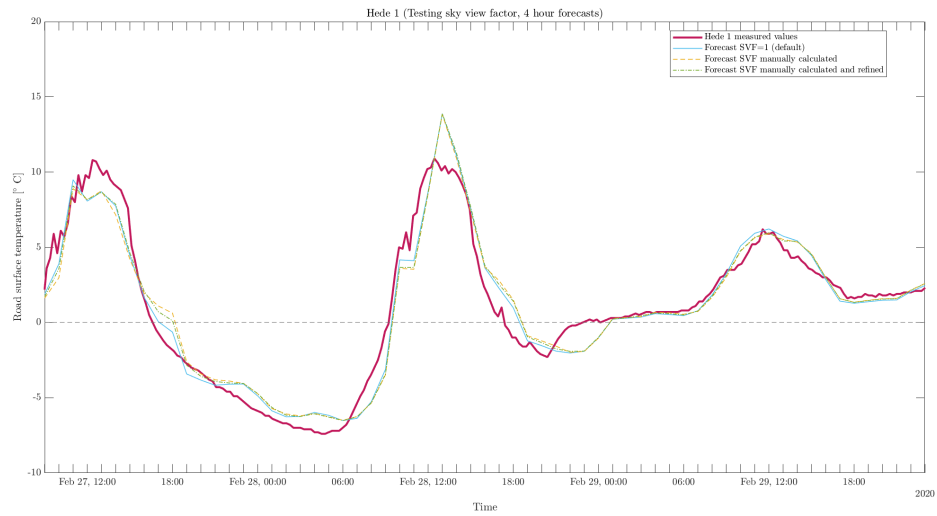


Figure 4.2: Plot with forecasts where the SVF parameter is modified around Hede station 1.

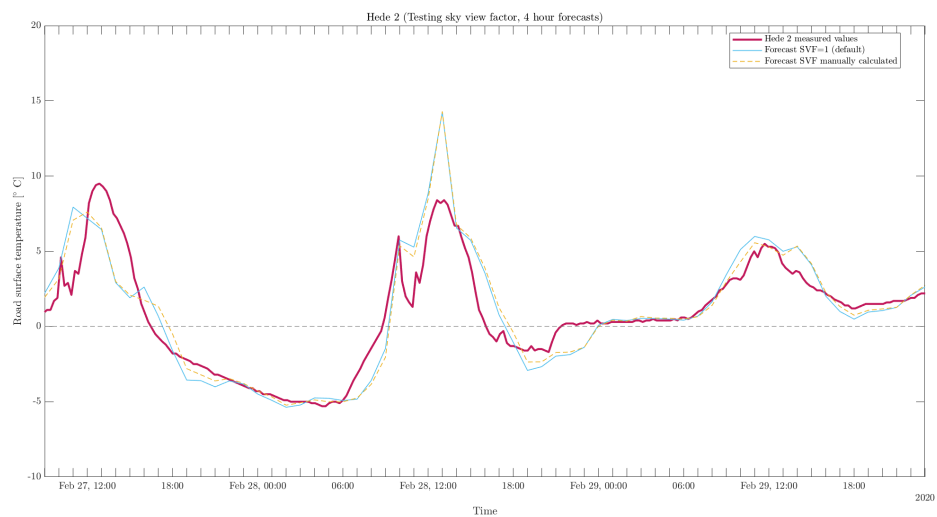


Figure 4.3: Plot with forecasts where the SVF parameter is modified around Hede station 2.

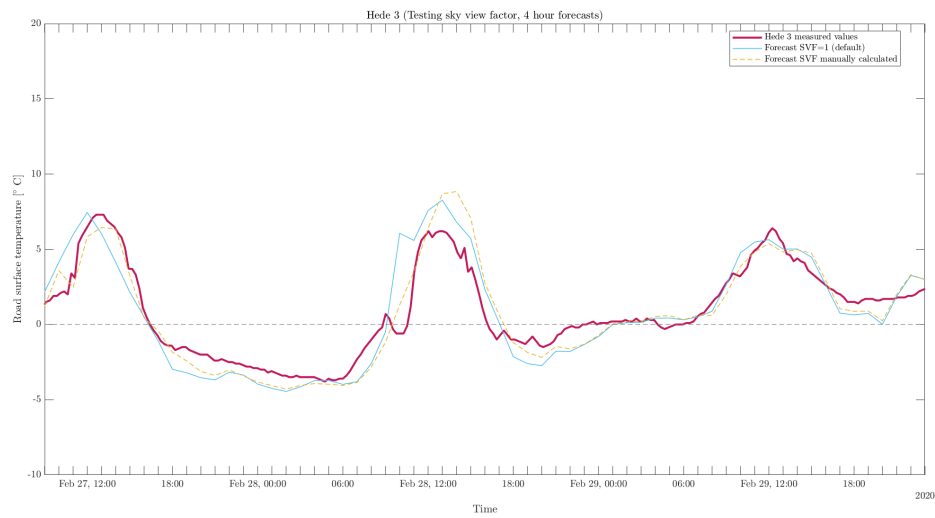


Figure 4.4: Plot with forecasts where the SVF parameter is modified around Hede station 3.

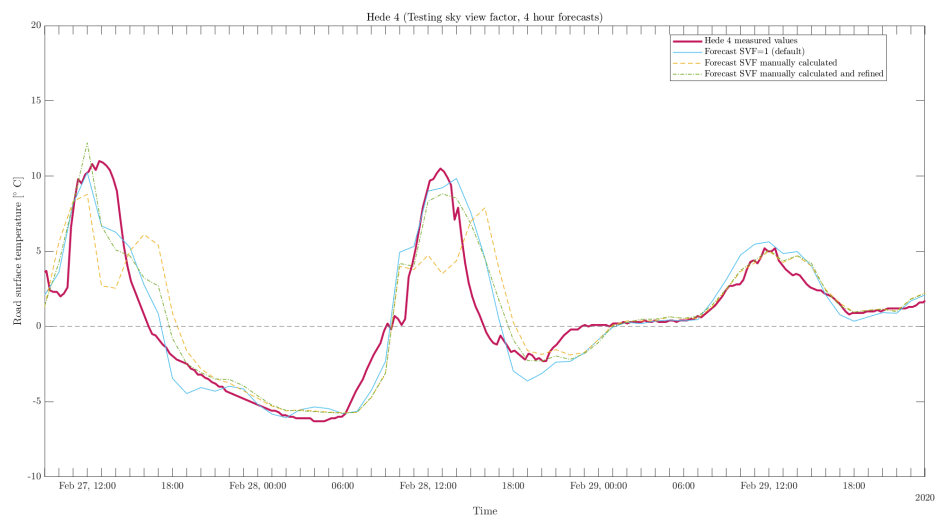


Figure 4.5: Plot with forecasts where the SVF parameter is modified around Hede station 4.

4. Results

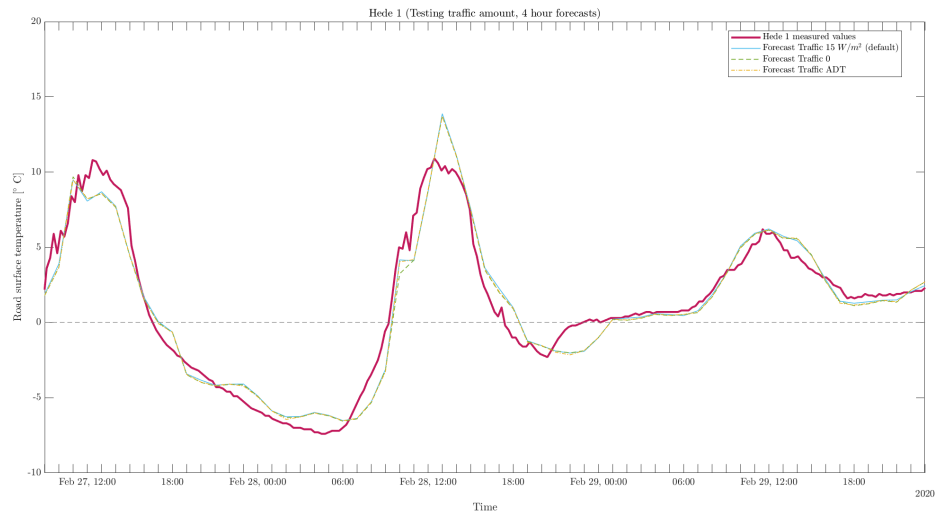


Figure 4.6: Plot with forecasts where the traffic amount parameter is modified around Hede 1.

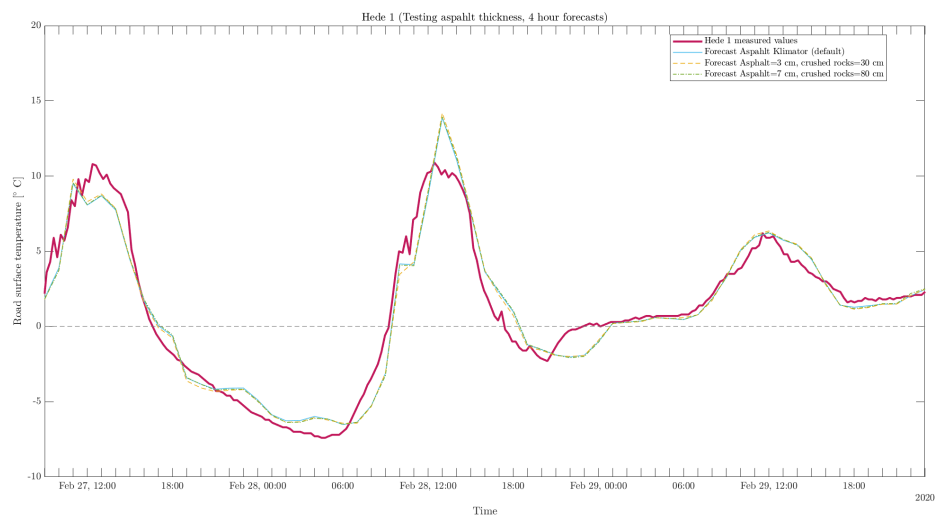


Figure 4.7: Plot with forecasts where the parameters thickness of the asphalt and the underlying layers are modified around Hede station 1.

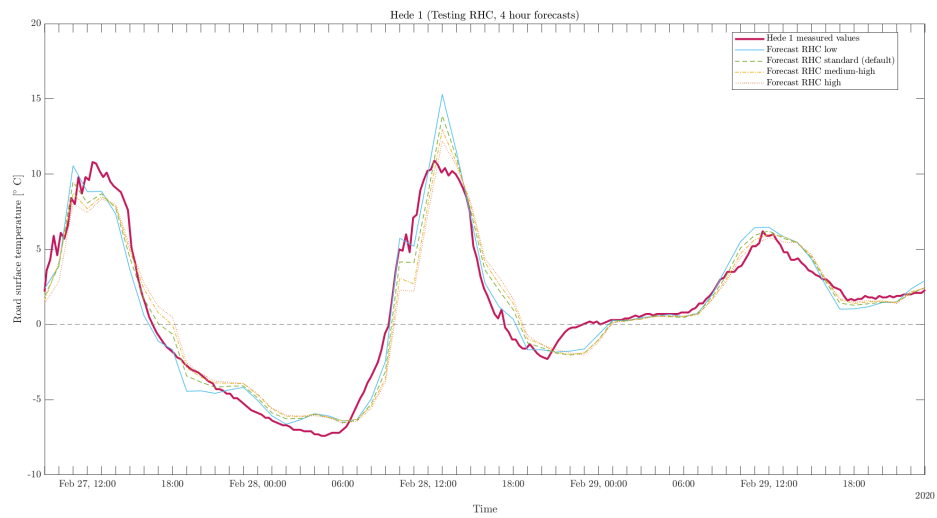


Figure 4.8: Plot with forecasts where the RHC parameter is modified around Hede station 1.

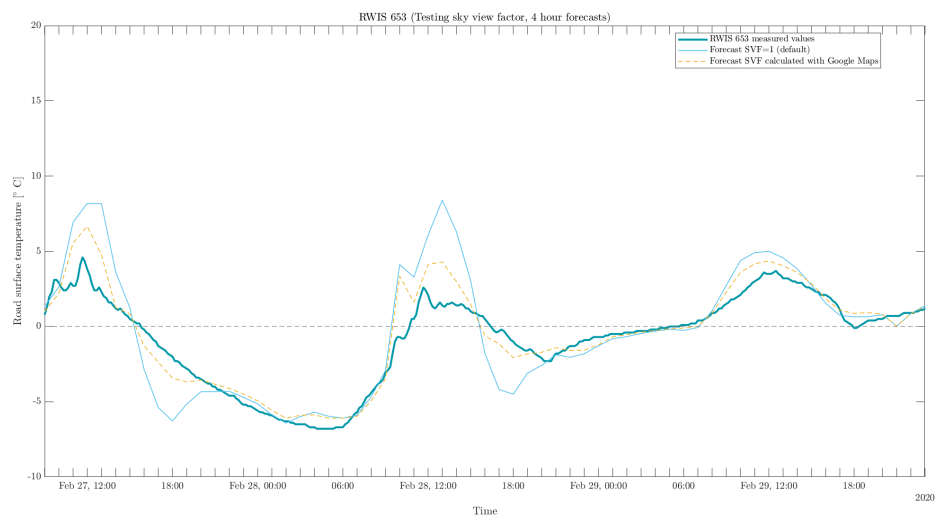


Figure 4.9: Plot with forecasts where the SVF parameter is modified around RWIS 653.

4. Results

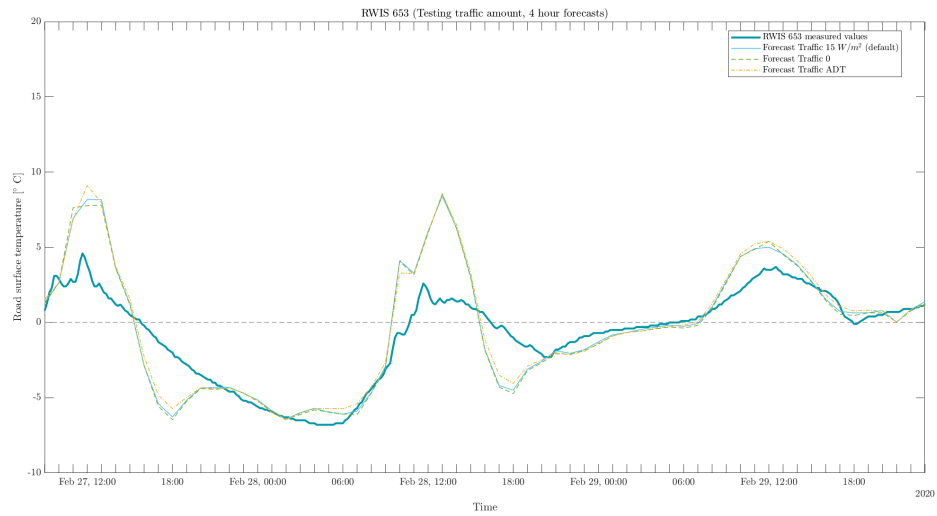


Figure 4.10: Plot with forecasts where the traffic amount parameter is modified around RWIS 653.

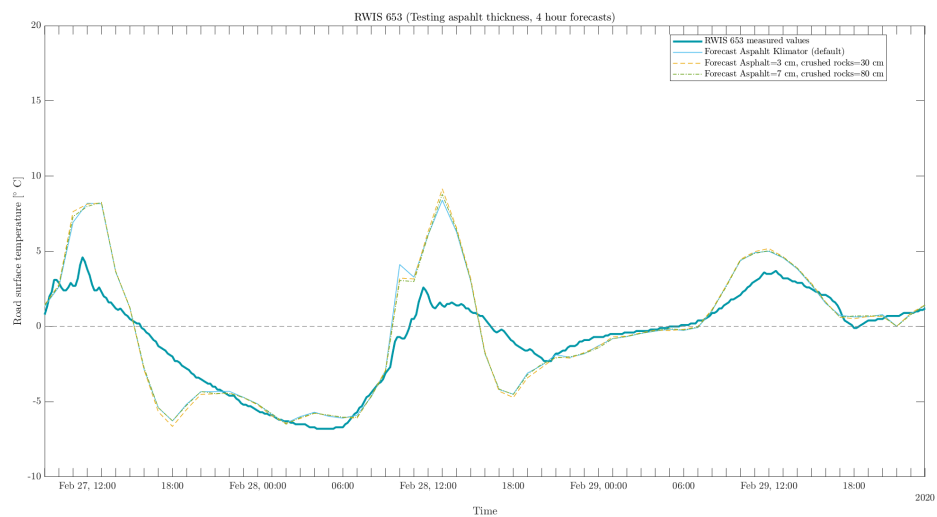


Figure 4.11: Plot with forecasts where the parameters thickness of the asphalt and the underlying layers are modified around RWIS 653.

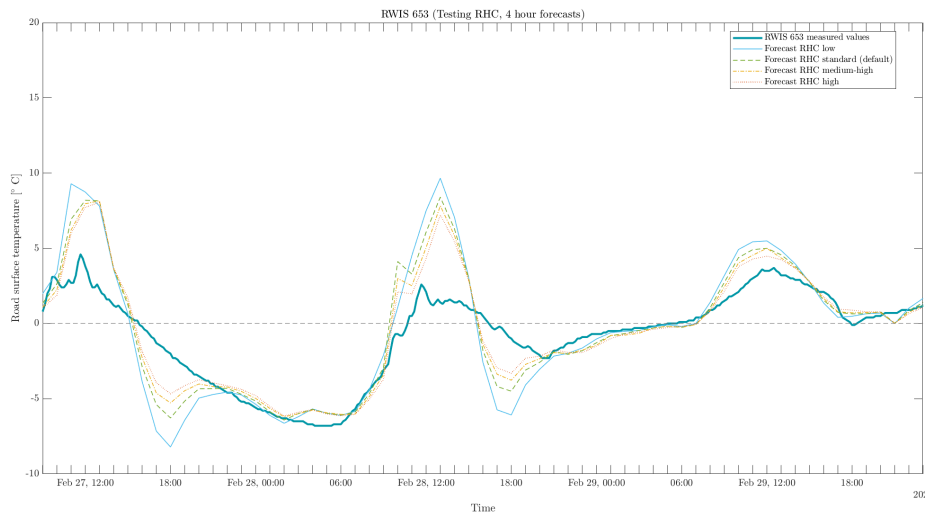


Figure 4.12: Plot with forecasts where the RHC parameter is modified around RWIS 653.

4.3 Tables and confusion matrices from the testing phase

In this section, the results from calculating the accuracy of the forecasts for the parameters modified in the testing phase, are presented. The section includes the results presented in section 3.2.6, and the added metrics made in retrospect to isolate scenarios that represent winter road maintenance and slip. The added metrics for the evaluation phase are MAE and RMSE for temperatures between 5 and -5°C and the difference between greatest and smallest error for each station. The results from calculating MAE and RMSE, both for all temperatures and for temperatures between 5 and -5°C , are compiled together in tables 4.3-4.18 for each parameter. The forecasts used in all calculations for this section, were 4-hour forecasts made on the whole test data set (February 27-29 and March 7-9). The calculations in tables 4.3-4.18 are made for the two intervals, all temperatures, and temperatures in between 5 to -5°C . In the tables the smallest error for each station is highlighted. In the tables, the italic values describe the difference between the greatest and smallest error for each station, and they are highlighted if they are $< 0.05^{\circ}\text{C}$.

In addition to this, table 4.19 presents the MAE and RMSE for the forecasts where the SVF parameter was modified, around the Hede stations, during sunrise. The forecasts used when calculating the errors in this table were 4-hour forecasts made on the whole test data set (February 27-29 and March 7-9). The calculations are made for the time interval 07:00-11:00 to show the effects of the SVF parameter during sunrise. In the table the smallest error for each station is highlighted.

4. Results

Table 4.3: The table presents the MAE for the forecasts where the SVF parameter was modified around the Hede stations.

Station	Temperature Interval	MAE Surface temperature [°C]			Δ MAE
		SVF manually calculated	SVF manually calculated and refined	SVF=1 (default)	
Hede 1	All temperatures	0,960	0,927	0,898	0,062
Hede 2	All temperatures	0,929	0,929	0,989	0,060
Hede 3	All temperatures	0,892	0,892	1,003	0,111
Hede 4	All temperatures	1,275	1,001	0,955	0,320
All Hede	All temperatures	1,014	0,938	0,961	0,076
Hede 1	5 to -5°C	0,933	0,895	0,814	0,119
Hede 2	5 to -5°C	0,907	0,907	0,849	0,058
Hede 3	5 to -5°C	0,807	0,807	0,882	0,075
Hede 4	5 to -5°C	1,255	0,980	0,953	0,302
All Hede	5 to -5°C	0,972	0,900	0,875	0,097

Table 4.4: The table presents the RMSE for the forecasts where the SVF parameter was modified, around the Hede stations.

Station	Temperature Interval	RMSE Surface temperature [°C]			Δ RMSE
		SVF manually calculated	SVF manually calculated and refined	SVF=1 (default)	
Hede 1	All temperatures	1,307	1,264	1,207	0,101
Hede 2	All temperatures	1,378	1,378	1,443	0,065
Hede 3	All temperatures	1,168	1,168	1,351	0,182
Hede 4	All temperatures	2,079	1,446	1,358	0,721
All Hede	All temperatures	1,525	1,318	1,342	0,206
Hede 1	5 to -5°C	1,247	1,192	1,076	0,171
Hede 2	5 to -5°C	1,262	1,262	1,164	0,098
Hede 3	5 to -5°C	1,002	1,002	1,064	0,062
Hede 4	5 to -5°C	2,042	1,393	1,301	0,742
All Hede	5 to -5°C	1,436	1,221	1,155	0,281

Table 4.5: The table presents the MAE for the forecasts where the SVF parameter was modified, around RWIS.

Station	Temperature Interval	MAE Surface temperature [°C]		Δ MAE
		SVF calculated with Google Maps	SVF=1 (default)	
RWIS 648	All temperatures	0,780	0,802	<i>0,022</i>
RWIS 651	All temperatures	0,610	1,018	<i>0,407</i>
RWIS 653	All temperatures	0,631	1,053	<i>0,422</i>
All RWIS	All temperatures	0,674	0,958	<i>0,284</i>
RWIS 648	5 to -5°C	0,686	0,692	<i>0,006</i>
RWIS 651	5 to -5°C	0,561	0,865	<i>0,304</i>
RWIS 653	5 to -5°C	0,615	0,775	<i>0,160</i>
All RWIS	5 to -5°C	0,616	0,782	<i>0,166</i>

Table 4.6: The table presents the RMSE for the forecasts where the SVF parameter was modified, around RWIS.

Station	Temperature Interval	RMSE Surface temperature [°C]		Δ RMSE
		SVF calculated with Google Maps	SVF=1 (default)	
RWIS 648	All temperatures	1,065	1,115	<i>0,051</i>
RWIS 651	All temperatures	0,889	1,490	<i>0,601</i>
RWIS 653	All temperatures	0,918	1,683	<i>0,765</i>
All RWIS	All temperatures	0,960	1,449	<i>0,488</i>
RWIS 648	5 to -5°C	0,817	0,831	<i>0,014</i>
RWIS 651	5 to -5°C	0,825	1,280	<i>0,455</i>
RWIS 653	5 to -5°C	0,891	1,178	<i>0,287</i>
All RWIS	5 to -5°C	0,846	1,125	<i>0,279</i>

Table 4.7: The table presents the MAE for the forecasts where the traffic amount parameter was modified, around the Hede stations.

Station	Temperature Interval	MAE Surface temperature [°C]			Δ MAE
		Traffic 0	Traffic 15 W/m ²	Traffic ÅDT	
Hede 1	All temperatures	0,918	0,898	0,911	0,020
Hede 2	All temperatures	0,979	0,989	0,985	0,010
Hede 3	All temperatures	1,012	1,003	1,021	0,018
Hede 4	All temperatures	0,952	0,955	0,951	0,003
All Hede	All temperatures	0,965	0,961	0,967	0,006
Hede 1	5 to -5°C	0,844	0,814	0,834	0,030
Hede 2	5 to -5°C	0,859	0,849	0,871	0,023
Hede 3	5 to -5°C	0,912	0,882	0,918	0,036
Hede 4	5 to -5°C	0,946	0,953	0,948	0,007
All Hede	5 to -5°C	0,891	0,875	0,894	0,019

Table 4.8: The table presents the RMSE for the forecasts where the traffic amount parameter was modified, around the Hede stations.

Station	Temperature Interval	RMSE Surface temperature [°C]			Δ RMSE
		Traffic 0	Traffic 15 W/m ²	Traffic ÅDT	
Hede 1	All temperatures	1,207	1,207	1,205	0,002
Hede 2	All temperatures	1,435	1,443	1,441	0,008
Hede 3	All temperatures	1,356	1,351	1,365	0,015
Hede 4	All temperatures	1,344	1,358	1,343	0,015
All Hede	All temperatures	1,339	1,342	1,341	0,003
Hede 1	5 to -5°C	1,080	1,076	1,077	0,004
Hede 2	5 to -5°C	1,171	1,164	1,184	0,020
Hede 3	5 to -5°C	1,104	1,064	1,108	0,044
Hede 4	5 to -5°C	1,282	1,301	1,282	0,019
All Hede	5 to -5°C	1,162	1,155	1,166	0,012

Table 4.9: The table presents the MAE for the forecasts where the traffic amount parameter was modified, around RWIS.

Station	Temperature Interval	MAE			Δ MAE
		Surface temperature [$^{\circ}$ C]			
		Traffic 0	Traffic 15 W/m^2	Traffic \dot{A} DT	
RWIS 648	All temperatures	0,818	0,802	0,818	0,016
RWIS 651	All temperatures	1,032	1,018	1,026	0,014
RWIS 653	All temperatures	1,066	1,053	1,062	0,013
All RWIS	All temperatures	0,972	0,958	0,969	0,014
RWIS 648	5 to -5° C	0,706	0,692	0,703	0,015
RWIS 651	5 to -5° C	0,877	0,865	0,782	0,095
RWIS 653	5 to -5° C	0,777	0,775	0,771	0,006
All RWIS	5 to -5°C	0,792	0,782	0,755	0,038

Table 4.10: The table presents the RMSE for the forecasts where the traffic amount parameter was modified, around RWIS.

Station	Temperature Interval	RMSE			Δ RMSE
		Surface temperature [$^{\circ}$ C]			
		Traffic 0	Traffic 15 W/m^2	Traffic \dot{A} DT	
RWIS 648	All temperatures	1,139	1,115	1,155	0,040
RWIS 651	All temperatures	1,523	1,490	1,484	0,039
RWIS 653	All temperatures	1,710	1,683	1,666	0,044
All RWIS	All temperatures	1,477	1,449	1,451	0,028
RWIS 648	5 to -5° C	0,869	0,831	0,832	0,038
RWIS 651	5 to -5° C	1,341	1,280	1,144	0,197
RWIS 653	5 to -5° C	1,182	1,178	1,152	0,031
All RWIS	5 to -5°C	1,162	1,125	1,063	0,099

4. Results

Table 4.11: The table presents the MAE for the forecasts where the asphalt and underlying layer thickness parameter was modified, around the Hede stations.

Station	Temperature Interval	MAE			Δ MAE
		Surface temperature [$^{\circ}$ C]			
		Asphalt 3 cm Crushed 30 cm	Asphalt 7 cm Crushed 80 cm	Asphalt Klimator (default)	
Hede 1	All temperatures	0,903	0,909	0,898	<i>0,011</i>
Hede 2	All temperatures	1,019	1,003	0,989	<i>0,030</i>
Hede 3	All temperatures	1,045	1,012	1,003	<i>0,041</i>
Hede 4	All temperatures	0,972	0,965	0,955	<i>0,017</i>
All Hede	All temperatures	0,985	0,972	0,961	<i>0,023</i>
Hede 1	5 to -5° C	0,806	0,830	0,814	<i>0,023</i>
Hede 2	5 to -5° C	0,874	0,873	0,849	<i>0,025</i>
Hede 3	5 to -5° C	0,922	0,898	0,882	<i>0,040</i>
Hede 4	5 to -5° C	0,904	0,907	0,953	<i>0,049</i>
All Hede	5 to -5°C	0,878	0,877	0,875	<i>0,003</i>

Table 4.12: The table presents the RMSE for the forecasts where the asphalt and underlying layer thickness parameter was modified, around the Hede stations.

Station	Temperature Interval	RMSE			Δ RMSE
		Surface temperature [$^{\circ}$ C]			
		Asphalt 3 cm Crushed 30 cm	Asphalt 7 cm Crushed 80 cm	Asphalt Klimator (default)	
Hede 1	All temperatures	1,213	1,223	1,207	<i>0,016</i>
Hede 2	All temperatures	1,497	1,461	1,443	<i>0,054</i>
Hede 3	All temperatures	1,410	1,361	1,351	<i>0,060</i>
Hede 4	All temperatures	1,391	1,372	1,358	<i>0,033</i>
All Hede	All temperatures	1,381	1,357	1,342	<i>0,039</i>
Hede 1	5 to -5° C	1,054	1,097	1,076	<i>0,043</i>
Hede 2	5 to -5° C	1,194	1,182	1,164	<i>0,030</i>
Hede 3	5 to -5° C	1,114	1,084	1,064	<i>0,050</i>
Hede 4	5 to -5° C	1,216	1,213	1,301	<i>0,087</i>
All Hede	5 to -5°C	1,147	1,145	1,155	<i>0,010</i>

Table 4.13: The table presents the MAE for the forecasts where the asphalt and underlying layer thickness parameter was modified, around RWIS.

Station	Temperature Interval	MAE			Δ MAE
		Surface temperature [°C]			
		Asphalt 3 cm Crushed 30 cm	Asphalt 7 cm Crushed 80 cm	Asphalt Klimator (default)	
RWIS 648	All temperatures	0,851	0,822	0,802	<i>0,049</i>
RWIS 651	All temperatures	1,100	1,024	1,018	<i>0,082</i>
RWIS 653	All temperatures	1,098	1,052	1,053	<i>0,046</i>
All RWIS	All temperatures	1,016	0,966	0,958	<i>0,059</i>
RWIS 648	5 to -5°C	0,729	0,697	0,692	<i>0,037</i>
RWIS 651	5 to -5°C	0,863	0,854	0,865	<i>0,011</i>
RWIS 653	5 to -5°C	0,773	0,751	0,775	<i>0,024</i>
All RWIS	5 to -5°C	0,793	0,773	0,782	<i>0,020</i>

Table 4.14: The table presents the RMSE for the forecasts where the asphalt and underlying layer thickness parameter was modified, around RWIS.

Station	Temperature Interval	RMSE			Δ RMSE
		Surface temperature [°C]			
		Asphalt 3 cm Crushed 30 cm	Asphalt 7 cm Crushed 80 cm	Asphalt Klimator (default)	
RWIS 648	All temperatures	1,194	1,149	1,115	<i>0,079</i>
RWIS 651	All temperatures	1,622	1,495	1,490	<i>0,132</i>
RWIS 653	All temperatures	1,761	1,683	1,683	<i>0,078</i>
All RWIS	All temperatures	1,544	1,459	1,449	<i>0,096</i>
RWIS 648	5 to -5°C	0,892	0,835	0,831	<i>0,061</i>
RWIS 651	5 to -5°C	1,240	1,261	1,280	<i>0,040</i>
RWIS 653	5 to -5°C	1,163	1,118	1,178	<i>0,060</i>
All RWIS	5 to -5°C	1,120	1,099	1,125	<i>0,026</i>

Table 4.15: The table presents the MAE for the forecasts where the RHC parameter was modified, around the Hede stations.

Station	Temperature Interval	MAE Surface temperature [°C]				Δ MAE
		RHC low	RHC standard (default)	RHC medium-high	RHC high	
Hede 1	All temperatures	0,874	0,898	0,968	1,030	0,132
Hede 2	All temperatures	1,120	0,989	0,965	0,940	0,049
Hede 3	All temperatures	1,175	1,003	0,929	0,886	0,117
Hede 4	All temperatures	1,022	0,955	0,957	0,985	0,031
All Hede	All temperatures	1,048	0,961	0,955	0,960	0,007
Hede 1	5 to -5°C	0,699	0,814	0,929	1,069	0,255
Hede 2	5 to -5°C	0,916	0,849	0,918	0,906	0,069
Hede 3	5 to -5°C	1,026	0,882	0,847	0,878	0,034
Hede 4	5 to -5°C	0,868	0,953	0,926	0,859	0,094
All Hede	5 to -5°C	0,882	0,875	0,904	0,925	0,049

Table 4.16: The table presents the RMSE for the forecasts where the RHC parameter was modified, around the Hede stations.

Station	Temperature Interval	RMSE Surface temperature [°C]				Δ RMSE
		RHC low	RHC standard (default)	RHC medium-high	RHC high	
Hede 1	All temperatures	1,215	1,207	1,309	1,407	0,201
Hede 2	All temperatures	1,659	1,443	1,374	1,343	0,317
Hede 3	All temperatures	1,643	1,351	1,234	1,174	0,469
Hede 4	All temperatures	1,450	1,358	1,370	1,440	0,092
All Hede	All temperatures	1,503	1,342	1,323	1,345	0,180
Hede 1	5 to -5°C	0,859	1,076	1,262	1,442	0,583
Hede 2	5 to -5°C	1,221	1,164	1,261	1,254	0,097
Hede 3	5 to -5°C	1,262	1,064	1,040	1,174	0,222
Hede 4	5 to -5°C	1,199	1,301	1,286	1,170	0,130
All Hede	5 to -5°C	1,152	1,155	1,215	1,260	0,108

Table 4.17: The table presents the MAE for the forecasts where the RHC parameter was modified, around RWIS.

Station	Temperature Interval	MAE				Δ MAE
		Surface temperature [°C]				
		RHC low	RHC standard (default)	RHC medium-high	RHC high	
RWIS 648	All temperatures	0,979	0,802	0,759	0,748	0,054
RWIS 651	All temperatures	1,352	1,018	0,831	0,717	0,300
RWIS 653	All temperatures	1,314	1,053	0,922	0,844	0,209
All RWIS	All temperatures	1,215	0,958	0,837	0,770	0,188
RWIS 648	5 to -5°C	0,804	0,692	0,666	0,655	0,037
RWIS 651	5 to -5°C	0,936	0,865	0,756	0,655	0,210
RWIS 653	5 to -5°C	0,780	0,775	0,726	0,721	0,054
All RWIS	5 to -5°C	0,844	0,782	0,719	0,677	0,105

Table 4.18: The table presents the RMSE for the forecasts where the RHC parameter was modified, around RWIS.

Station	Temperature Interval	RMSE				Δ RMSE
		Surface temperature [°C]				
		RHC low	RHC standard (default)	RHC medium-high	RHC high	
RWIS 648	All temperatures	1,426	1,115	1,006	0,968	0,458
RWIS 651	All temperatures	1,978	1,490	1,197	1,023	0,955
RWIS 653	All temperatures	2,096	1,683	1,461	1,316	0,780
All RWIS	All temperatures	1,856	1,449	1,236	1,113	0,743
RWIS 648	5 to -5°C	1,047	0,831	0,790	0,797	0,257
RWIS 651	5 to -5°C	1,346	1,280	1,130	0,958	0,389
RWIS 653	5 to -5°C	1,129	1,178	1,048	0,993	0,185
All RWIS	5 to -5°C	1,190	1,125	1,011	0,926	0,264

Table 4.19: The table presents the MAE and RMSE for the forecasts where the SVF parameter was modified, around the Hede stations, during sunrise. The forecasts used when calculating the errors were 4-hour forecasts made on the whole test data set (February 27-29 and March 7-9). The calculations are made for the time interval 07:00-11:00 to show the effects of the SVF parameter during sunrise. In the table the smallest errors for each station are highlighted.

Station	Time Interval	MAE Surface temperature [°C]		RMSE Surface temperature [°C]	
		SVF manually calculated and refined	SVF=1 (default)	SVF manually calculated and refined	SVF=1 (default)
Hede 1	07:00-11:00	1,532	1,335	1,902	1,706
Hede 2	07:00-11:00	1,185	1,158	1,401	1,332
Hede 3	07:00-11:00	1,396	1,489	1,585	2,076
Hede 4	07:00-11:00	1,707	1,374	2,079	1,774
All Hede	07:00-11:00	1,455	1,339	1,762	1,742

4.4 Confusion matrices from the testing phase

In this section the confusion matrices calculated for the extended analysis of the testing phase are presented. The confusion matrices have the condition positive for temperatures above 0°C. In the matrices, the green values represent when the forecasts and measured values agree with each other; the yellow values represent the false negatives, and the red value represents the false positives. In the matrices, different rates are calculated based on the formulas in figure 2.9. The calculations are made on 4-hour forecasts made on the whole test data set (February 27-29 and March 7-9).

		Actual Values			
		Positive (0)	Negative (1)		
Predicted Values	Positive (1)	586	33	True Positive Rate (TPR): 94.7 %	False Positive Rate (FPR): 8.7 %
	Negative (0)	33	345	False Negative Rate (FNR): 5.3 %	True Negative Rate (TNR): 91.3 %
		Total population: 997		Accuracy = 93.4 %	

(a) The confusion matrix for when the RHC parameter was set to a low value around the Hede stations.

		Actual Values			
		Positive (0)	Negative (1)		
Predicted Values	Positive (1)	586	33	True Positive Rate (TPR): 93.6 %	False Positive Rate (FPR): 8.9 %
	Negative (0)	40	338	False Negative Rate (FNR): 6.4 %	True Negative Rate (TNR): 91.1 %
		Total population: 997		Accuracy = 92.7 %	

(b) The confusion matrix for when the RHC parameter was set to the default standard value around the Hede stations.

		Actual Values			
		Positive (0)	Negative (1)		
Predicted Values	Positive (1)	585	34	True Positive Rate (TPR): 92.4 %	False Positive Rate (FPR): 9.3 %
	Negative (0)	48	330	False Negative Rate (FNR): 7.6 %	True Negative Rate (TNR): 90.7 %
		Total population: 997		Accuracy = 91.8 %	

(c) The confusion matrix for when the RHC parameter was set to a medium-high value around the Hede stations.

		Actual Values			
		Positive (0)	Negative (1)		
Predicted Values	Positive (1)	583	36	True Positive Rate (TPR): 92.1 %	False Positive Rate (FPR): 9.9 %
	Negative (0)	50	328	False Negative Rate (FNR): 7.9 %	True Negative Rate (TNR): 90.1 %
		Total population: 997		Accuracy = 91.4 %	

(d) The confusion matrix for when the RHC parameter was set to a high value around the Hede stations.

Figure 4.13: The figures show the confusion matrices for when the RHC parameter was modified on the test data set around the Hede stations.

4. Results

		Actual Values			
		Positive (0)	Negative (1)		
Predicted Values	Positive (1)	523	61	True Positive Rate (TPR): 91.3 %	False Positive Rate (FPR): 11.1 %
	Negative (0)	50	490	False Negative Rate (FNR): 8.7 %	True Negative Rate (TNR): 88.9 %
Total population: 1124		Accuracy = 90.1 %			

(a) The confusion matrix for when the RHC parameter was set to a low value around RWIS.

		Actual Values			
		Positive (0)	Negative (1)		
Predicted Values	Positive (1)	524	60	True Positive Rate (TPR): 91.8 %	False Positive Rate (FPR): 10.8 %
	Negative (0)	47	493	False Negative Rate (FNR): 8.2 %	True Negative Rate (TNR): 89.2 %
Total population: 1124		Accuracy = 90.5 %			

(b) The confusion matrix for when the RHC parameter was set to the default standard value around RWIS.

		Actual Values			
		Positive (0)	Negative (1)		
Predicted Values	Positive (1)	585	34	True Positive Rate (TPR): 92.4 %	False Positive Rate (FPR): 9.3 %
	Negative (0)	48	330	False Negative Rate (FNR): 7.6 %	True Negative Rate (TNR): 90.7 %
Total population: 997		Accuracy = 91.8 %			

(c) The confusion matrix for when the RHC parameter was set to a medium-high value around RWIS.

		Actual Values			
		Positive (0)	Negative (1)		
Predicted Values	Positive (1)	537	47	True Positive Rate (TPR): 91.5 %	False Positive Rate (FPR): 8.8 %
	Negative (0)	50	490	False Negative Rate (FNR): 8.5 %	True Negative Rate (TNR): 91.2 %
Total population: 1124		Accuracy = 91.4 %			

(d) The confusion matrix for when the RHC parameter was set to a high value around RWIS.

Figure 4.14: The figures show the confusion matrices for when the RHC parameter was modified on the test data set around RWIS.

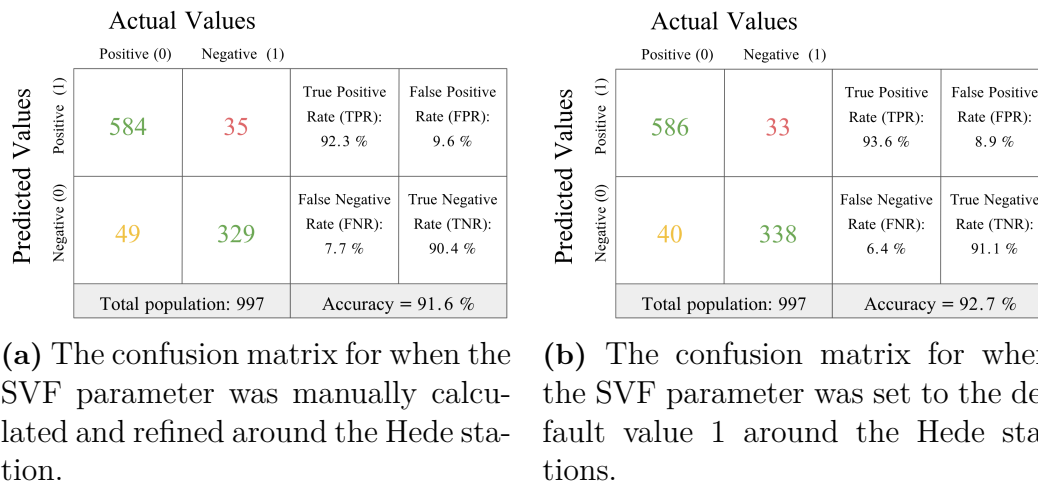


Figure 4.15: The figures show the confusion matrices for when the SVF parameter was modified on the test data set around Hede.

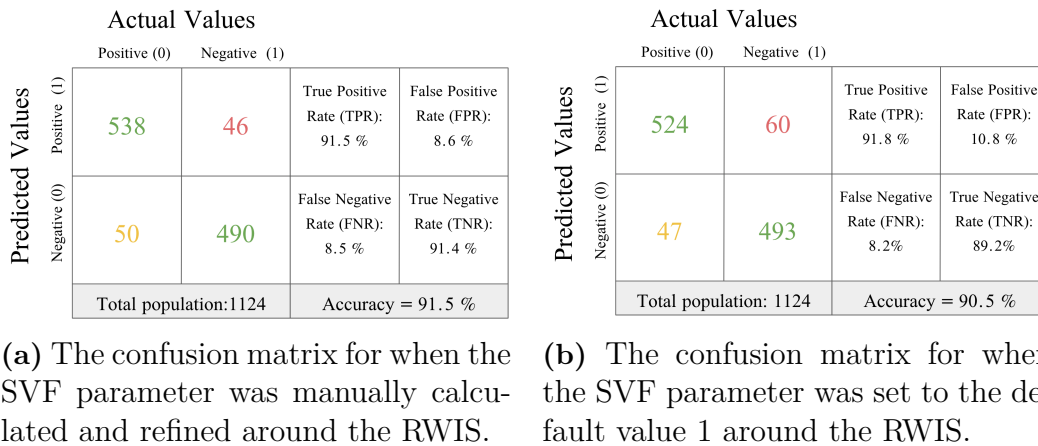


Figure 4.16: The figures show the confusion matrices for when the SVF parameter was modified on the test data set around RWIS.

4.5 Plots, tables, and confusion matrices from the validation phase

In this section, selected results from the validation phase are presented in plots, tables and confusion matrices. For the same reason as in section 4.2, only plots for Hede 1 and RWIS 653 will be presented. The results below are from forecasts made on the whole validation data set, February 27-March 27.

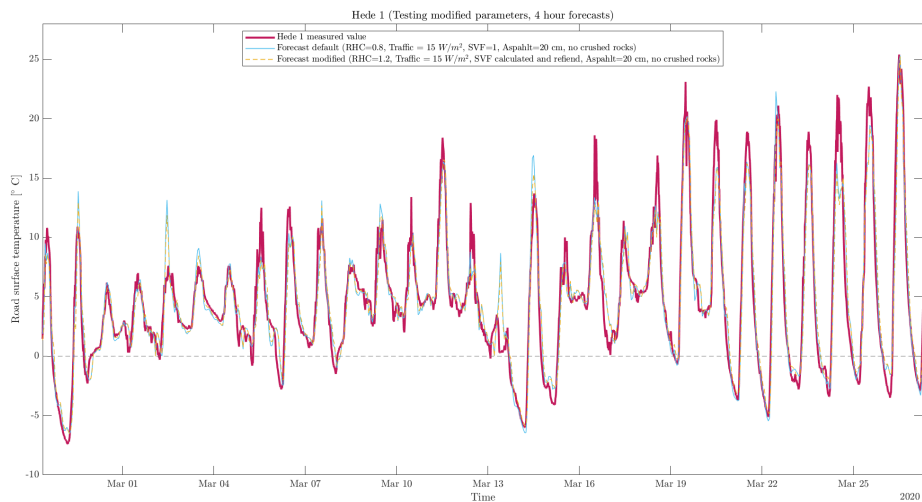


Figure 4.17: Plot with measured values and 4-hour forecasts where the SVF and RHC parameters has been modified around Hede 1. The plots shows measured values and forecasts made on February 27-March 27.

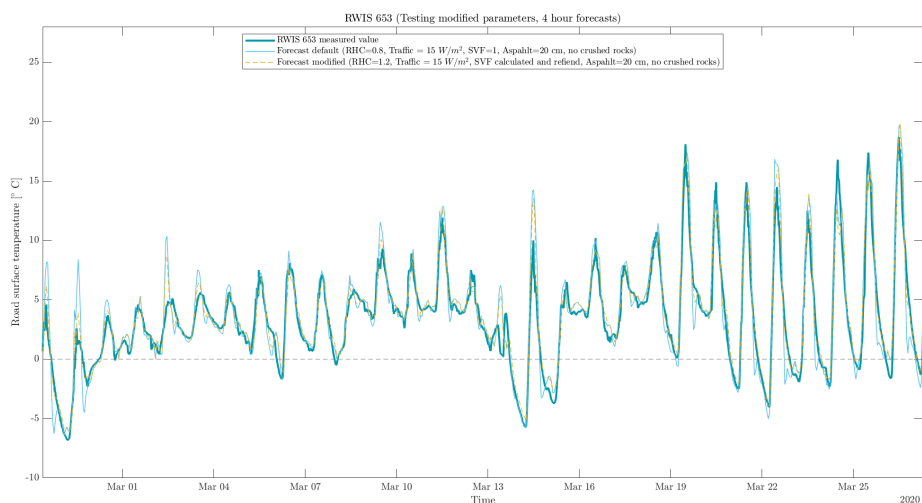


Figure 4.18: Plot with measured values and 4-hour forecasts where the SVF and RHC parameters has been modified around RWIS 653. The plots shows measured values and forecasts made on February 27-March 27.

		Actual Values			
		Positive (0)	Negative (1)		
Predicted Values	Positive (1)	8897	146	True Positive Rate (TPR): 97.1 %	False Positive Rate (FPR): 7.7 %
	Negative (0)	264	1752	False Negative Rate (FNR): 2.9 %	True Negative Rate (TNR): 92.3 %
Total population: 11059				Accuracy = 96.3 %	

		Actual Values			
		Positive (0)	Negative (1)		
Predicted Values	Positive (1)	8915	128	True Positive Rate (TPR): 95.5 %	False Positive Rate (FPR): 7.4 %
	Negative (0)	421	1595	False Negative Rate (FNR): 4.5 %	True Negative Rate (TNR): 92.6 %
Total population: 11059				Accuracy = 95.0 %	

(a) The confusion matrix for when the default values were used around the Hede stations.

(b) The confusion matrix for when the SVF and RHC parameters were modified around the Hede stations.

Figure 4.19: The figures show the confusion matrices for when the default and modified values were used on the validation data set around the Hede stations. In the matrices, the green values represent when the forecasts and measured values agree with each other; the yellow values represent the false negatives, and the red value represents the false positives. In the matrices, different rates are calculated based on the formulas in figure 2.9

		Actual Values			
		Positive (0)	Negative (1)		
Predicted Values	Positive (1)	9742	286	True Positive Rate (TPR): 96.8 %	False Positive Rate (FPR): 12.9 %
	Negative (0)	326	1923	False Negative Rate (FNR): 3.2 %	True Negative Rate (TNR): 87.1 %
Total population: 12277				Accuracy = 95.0 %	

		Actual Values			
		Positive (0)	Negative (1)		
Predicted Values	Positive (1)	9940	88	True Positive Rate (TPR): 96.2 %	False Positive Rate (FPR): 4.5 %
	Negative (0)	398	1851	False Negative Rate (FNR): 3.8 %	True Negative Rate (TNR): 95.5 %
Total population: 12277				Accuracy = 96.0 %	

(a) The confusion matrix for when the default values were used around the RWIS.

(b) The confusion matrix for when the SVF and RHC parameters were modified around the RWIS.

Figure 4.20: The figures show the confusion matrices for when the default and modified values were used on the validation data set around the RWIS. In the matrices, the green values represent when the forecasts and measured values agree with each other; the yellow values represent the false negatives, and the red value represents the false positives. In the matrices, different rates are calculated based on the formulas in figure 2.9

4. Results

Table 4.20: The table presents MAE and RMSE for forecasts made on Hede stations where the SVF and RHC parameters were modified, and for when default values were used on all parameters. The forecasts used when calculating the errors were 4-hour forecasts made on the validation data set (February 27-March 27). The calculations were made on all temperatures, the temperature interval 5 to -5°C , and the temperature interval 2 to -2°C .

Station	Temperature Interval	MAE Surface temp		RMSE Surface temp	
		Default	Modified	Default	Modified
Hede 1	All temperatures	1,129	1,273	1,616	1,763
Hede 2	All temperatures	1,262	1,426	1,937	2,225
Hede 3	All temperatures	1,122	1,415	1,628	2,456
Hede 4	All temperatures	1,172	1,610	1,704	2,390
All Hede	All temperatures	1,171	1,431	1,726	2,225
Hede 1	5 to -5°C	0,814	1,057	1,076	1,435
Hede 2	5 to -5°C	0,849	0,923	1,164	1,307
Hede 3	5 to -5°C	0,882	0,821	1,064	1,044
Hede 4	5 to -5°C	0,953	1,047	1,301	1,474
All Hede	5 to -5°C	0,875	0,957	1,155	1,320

Table 4.21: The table presents MAE and RMSE for forecasts made on RWIS stations where the SVF and RHC parameters were modified, and for when default values were used on all parameters. The forecasts used when calculating the errors were 4-hour forecasts made on the validation data set (February 27-March 27). The calculations were made on all temperatures, the temperature interval 5 to -5°C , and the temperature interval 2 to -2°C .

Station	Temperature Interval	MAE Surface temp		RMSE Surface temp	
		Default	Modified	Default	Modified
RWIS 648	All temperatures	0,991	0,854	1,454	1,221
RWIS 651	All temperatures	1,346	0,784	2,170	1,299
RWIS 653	All temperatures	1,081	0,763	1,603	1,097
All RWIS	All temperatures	1,139	0,800	1,769	1,209
RWIS 648	5 to -5°C	0,692	0,662	0,831	0,811
RWIS 651	5 to -5°C	0,865	0,503	1,280	0,702
RWIS 653	5 to -5°C	0,775	0,593	1,178	0,788
All RWIS	5 to -5°C	0,782	0,580	1,125	0,764

5

Discussion

In this chapter, the methods and results will be discussed in order to answer the research questions of the project. The discussion is divided into the sections analyzing the results from the testing phase, analyzing the results from the validation phase, and lastly, evaluation of the method. Research questions 2 and 3 (RQ.2 and RQ.3) are discussed by analyzing the results in sections 5.1 and 5.2. In section 5.1, an extended analysis regarding each parameter through the results from the testing phase will be presented to give a deeper understanding of how each parameter might affect the climate model. In section 5.2, the results from the validation phase will be discussed to see if any results from the testing phase can be validated. Research question 1 (RQ.1) is continuously discussed throughout the two sections 5.1 and 5.2, where the results regarding differences between car-borne roads and bicycle paths, presented in section 4.1, and how these differences are reflected in the result, are discussed. Lastly, the method used throughout the project will be discussed to highlight the strengths and insecurities of the method. The discussions are summarized in chapter 6 through conclusion and recommendations.

5.1 Analyzing the results from the testing phase

In this section, the results from the testing presented in the evaluation phase, and further analysis for each parameter, are discussed. When analyzing the results, it can be seen that some parameters affect the behavior of the forecasts more than others. The parameters that do not seem to change the behavior of the forecasts are traffic amount and thickness of the asphalt and underlying layers. These two parameters also have a profound effect on the accuracy of the forecasts. The parameters SVF and RHC, on the other hand, seem to affect both the behavior and improve the accuracy of the forecasts. The significance of each parameter when it comes to changing the behavior and improving accuracy is described in the sections below.

Before doing a detailed analysis of each parameter, there are a couple of things listed below that should be noted.

- In the testing phase the parameters were tested over a short period, consisting of 6 days, and therefore no certain conclusions can be drawn from these results.

- The temperatures in the months where the parameters have been tested are generally higher than during the colder winter months for which the climate model is constructed.
- The measured temperatures varies between the different Hede stations, see figure 4.1. This was intended when selecting the positions of the Hede stations to get a varied data set, and is a result of the differences in the microclimates.
- When comparing the results from bicycle paths and car-borne roads, it can be seen that the measured temperatures on the car-borne roads are generally lower than the temperatures for bicycle paths, see figure 4.1. Because of the small data set used during testing, no discussion about how the temperature difference affect the results will be made.

5.1.1 Analyzing traffic amount

The results from RQ.1, presented in section 4.1, shows that when comparing traffic amount for car-borne roads and bicycle-path there is a significant difference in reality, see table 4.1. However, looking at the plot in figure 4.10, no notable difference between the forecast when traffic is modified to 0, and the forecast when traffic is modified according to ÅDT in table 4.1 can be seen. The figure shows that the forecasts follow approximately the same curve independently of the tested parameter values, with small differences in magnitude. The same can be seen in figure 4.6, with forecasts around Hede 1, where the difference is even smaller since there is little traffic on bicycle paths.

By further analyzing the MAE and RMSE in the tables, 4.7 and 4.8 it can be confirmed that the accuracy of the default and modified parameter values for traffic does not differ much. Since the difference in MAE and RMSE for the forecasts with modified traffic amount is < 0.05 around Hede stations, see tables 4.7 and 4.8, the traffic amount parameter is concluded to be of less importance for bicycle paths. However, by analyzing the plot in figure 4.6 at 9 o'clock, it can be seen that the climate model can react to small changes. At 9 o'clock, the forecasts with default traffic amount and traffic amount set to ÅDT for bicycles seen in table 4.1, gives almost the same temperature. Nevertheless, when traffic is set to 0, the temperature becomes slightly lower. Since the parameter traffic amount does not significantly affect the climate model's accuracy, based on the testing phase, it is not recommended to prioritize further testing and the tuning of this parameter.

When estimating the amount of traffic on bicycle paths a lot of assumptions were made. But since the traffic amount parameter does not affect the climate model significantly, the assumptions has not affected the results of this project negatively.

5.1.2 Analyzing thickness of the asphalt and underlying layers

According to the results from RQ.1, seen in 4.1, the thickness of the asphalt and the underlying layers might differ between car-borne roads and bicycle paths as a result of bicycle paths being constructed for lower loads. However, similar to traffic, it can be seen in figures 4.7 and 4.11, that modifying the thickness of the asphalt and the underlying layers do not affect the resulting forecasts significantly. By analyzing the calculations for MAE and RMSE in the tables, 4.11-4.14, it can be confirmed that the differences between the changed parameter values are small. The differences for MAE are < 0.05 for all Hede and most RWIS, and the differences for RMSE are also relatively small. The small differences in errors in combinations with the small changes in the plots, lead to the conclusion that asphalt thickness is not seen as a significant parameter when modifying the climate model to fit bicycle paths. However, similar to traffic amount, it can be seen in 4.7 at 9 o'clock that the climate model can react to small changes regarding asphalt thickness as well, and that the climate model could benefit from improving the parameter and test the modifications on a more extensive data set. Since the asphalt thickness parameter asphalt thickness does not affect the accuracy of the climate model significantly, it is not recommended to prioritize further testing and the tuning of this parameter.

5.1.3 Analyzing SVF

When answering RQ.1 in section 4.1, it is explained that the calculation method for the SVF parameter differs between car-borne roads and bicycle paths. The results from modifying the SVF parameter will be discussed in this section.

Unlike the forecasts where traffic amount and asphalt thickness was modified, it can be seen in figures 4.2-4.9 that the SVF parameter makes a notable difference for the forecasts. The effect of the SVF parameter is also shown in tables 4.3-4.6, where the differences in errors are > 0.05 for all Hede stations and most of the RWIS as well.

The significance of the SVF parameter becomes especially apparent when analyzing figure 4.5, showing surface temperature forecasts around Hede station 4. For Hede station 4, the SVF parameter was calculated in two iterations, the first is called SVF manually calculated, and the second is called SVF manually calculated and refined. In the figure 4.5, it can be seen that the first iteration, SVF manually calculated, deviates from the measured values in the middle of the day, during February 27 and 28, as a result of shadows created on the road from the horizontal angles. The dip is corrected in the second iteration, SVF manually calculated and refined, where the shadows were removed for the solar angles corresponding to the hours where the dip appeared. The difference in result in between the two iterations of SVF shows that a small modification in the SVF parameter can lead to great change in the behavior of the forecasts.

The forecasts in figure 4.5 does also exemplify how SVF, unlike the other parameters, can be adjusted for certain solar angles, i.e., certain times of the day. In other words,

SVF can modify isolated instances of the forecasts, while a modification of the other parameters rather creates a continuous change for the entire forecast. This property of the parameter, combined with the SVF's ability to be set for the specific position, creates the possibility to adapt the horizontal angle by using a set of measured values as reference. However, to adapt the SVF parameter and the horizontal angles in retrospect, can demand much work and does not guarantee a better result than using default $SVF=1$. The difficulty to adapt the SVF parameter becomes clear when analyzing MAE and RMSE for both Hede 1 and Hede 4, see tables 4.3 - 4.4, where the adjustments made for the refined SVF improves the results, but the errors for $SVF=1$ are still lower.

The results from Hede stations 3 and 4 exemplifies the importance of a high-quality manual calculation for the SVF and that the SVF parameter does affect the accuracy of the forecasts. By comparing the plots in the figures 4.4 and 4.5, it can be seen that manually calculating the parameter SVF can lead to both great improvements as well as deterioration. The improvements of a well manually calculated SVF can be seen when analyzing Hede station 3. In figure 4.4, it can be seen that the surface temperature forecasts with SVF manually calculated are closer to the measured value, especially in the forenoon. This is attested by tables 4.3 and 4.4, where it can be seen that the errors for the forecasts with manually calculated SVF around Hede 3 are smaller compared to having default SVF. The deterioration of an inaccurate manually calculated SVF can be seen when analyzing Hede station 4, where the surface temperature forecast with inaccurate calculated SVF deviated from the measured values in the middle of the day. As seen in tables 4.3 and 4.4, an inaccurate SVF leads to significantly higher errors compared to having the default value $SVF=1$ for Hede 4.

When analyzing the road surface temperature forecast around RWIS with SVF modified, the significance of an accurate SVF becomes even clearer. In tables 4.5 and 4.6 it can be seen that when using SVF calculated with street view in Google Maps the results improve significantly for all RWIS. The results are unanimous for all stations on both temperature intervals analyzed. It is also confirmed by the confusion matrices in figure 4.16 where the accuracy is improved, and the number of false positives decreases. The results from RWIS show a strong indication that SVF calculated with street view improves the results compared to using open sky, even if it is tested on a small data set.

Contrary to the results from RWIS, the results from Hede are more widespread, making it difficult to conclude which parameter value is the best. At first glance, it may seem that the refined value is best, which was the value selected from the evaluation phase. However, when extending the analysis for a temperature range closer to zero degrees, 5 to -5°C , $SVF=1$ gives lower errors instead. As described in section 3.2.2, it is critical that SVF is well calculated for sunrise and sunset, since a poorly calculated SVF can create an offset in the timing of the sunrise or sunset. The effects on sunrise are confirmed by table 4.19, where the manually calculated SVF gives higher errors for the hour when sunrise occurs. The confusion matrices in 4.15 also indicate that the default SVF gives slightly better accuracy and slightly

fewer false positives.

Since these analyses are made on a small-time interval, it can not be concluded which parameter is best for bicycle paths. There are indications that SVF is of great importance for the result, and should be further tested on a larger time interval. It also appears that the RWIS method gives a distinct result, in terms of accuracy, and therefore, a similar method should be developed for bicycle paths and tested against default. Since the parameter SVF does affect the accuracy of the climate model significantly, it is recommended to prioritize further testing of this parameter. Based on the result, it is recommended to further develop a method for calculating the SVF parameter in detail, similar to the method used for car-borne roads. It is recommended to test and validate the modification of SVF on a more considerable period for both bicycle paths and car-borne roads, and preferably on data collected during the colder winter months.

5.1.4 Analyzing road heat conductivity

The results from RQ.1, presented in section 4.1, shows that different type of asphalt might be used when constructing bicycle paths, leading to the RHC parameter being affected. The results from modifying the RHC parameter will be discussed in this section.

By looking at the plots in figures 4.8 and 4.12, it can be seen that the forecasts with RHC modified differs from each other. It is especially clear when looking at the peaks as well as the afternoon on February 28 in figure 4.8, where all forecasts are distinct. That the forecasts differ from each other indicates that the RHC parameter is of relevance. By analyzing the tables 4.15, it can be seen that the difference in MAE is > 0.05 for some Hede stations and smaller for others, but unlike asphalt, the RMSE table 4.16 shows that the differences can become significant when weighing in large errors. The differences in RMSE for Hede in combination with the significant differences in errors for RWIS, shown in tables 4.17 and 4.18, indicates that the RHC parameter is of significance.

By further analyzing the plots in figures 4.8 and 4.12, it can be seen that the RHC parameter influence how fast the surface is heated and cooled down. This is visualized in figure 4.12, where the forecast with a low value on RHC, have distinct peaks and valleys. In theory, a low value on RHC, corresponds to porous asphalt, meaning that less heat is transferred to the ground. The surface does then become heated faster, meaning that the results in the plots agree well with theory. What can be further noted, is that the RHC parameter is suitable to improve the accuracy of the forecasts' general behavior, in comparison to SVF, which is useful for isolating certain instances of the forecast.

When analyzing the tables 4.15, 4.16, and confusions matrices in figure 4.13, for Hede it can be seen that there is no clear result regarding which parameter value that is the best fitted for bicycle paths. Since the results for the RHC parameter around the Hede stations are widespread, no conclusions regarding which RHC value

that should be used for bicycle paths can be drawn. However, some tendencies can be spotted when comparing the results from RWIS made on car-borne roads with the results from Hede made on bicycle paths. In tables 4.17 and 4.18, it can be seen that the errors become smaller for higher values on the RHC parameter on the car-borne roads tested for all stations as well as for both temperature intervals, and the results from the confusion matrices in figure 4.14, indicate that the medium-high value on the RHC parameter leads to higher accuracy and less false positive values for RWIS. All results regarding RWIS indicate that higher values on RHC, such as medium-high or high, lead to improvements for car-borne roads. Bicycle-paths, in contrast to car-borne roads, do not show the clear tendencies that a higher RHC value gives a consistent better result. Instead, it varies between the lower and medium values, depending on the temperature range and station position. Therefore, further investigation should be made on these lower RHC values. Using a different RHC on bicycle paths is also inline with the results from RQ.1, presented in section 4.1, where it is described that the priorities regarding e.g., flexibility for bicycle paths might lead to different asphalt being used when constructing bicycle paths. Secondly, it is recommended to test higher values on RHC to confirm how these affect the climate model for bicycle paths. Since the parameter RHC does affect the accuracy of the climate model significantly, it is recommended to prioritize further testing and the tuning of this parameter. It is recommended to test lower values on RHC for bicycle paths on a larger period, preferably on data collected during the colder winter months, and compare with results from the test made on car-borne roads.

5.2 Analyzing the results from the validation phase

In this section, the results from the validation phase are analyzed and discussed. The default values in this section are SVF being set to 1, traffic amount is set to $15 \frac{W}{m^2}$, asphalt thickness set by Klimator, and RHC is set to standard. For the modified parameters, SVF is calculated manually for Hede and with Google Maps for RWIS, and RHC is set to medium. Traffic amount and asphalt thickness are set to the same values as for default. The default and modified values are further described in chapter 3. The results in this section are from tests made on the validation data set, consisting of data from February 27-March 27, visualized in figures 4.17 and 4.18. In the figures, it can be seen that both forecast with the default and modified parameters, seem to follow the measured values well.

When analyzing the results from the validation phase, it can be seen that the results did not match the results from the first evaluation phase made in 3.2.6. In the evaluation phase it seemed that SVF manually calculated and refined, and RHC medium-high would lead to better results for the Hede stations, but this is not the case in the validation phase. In table 4.20, it can be seen that the errors are smaller for default values, for both temperature intervals. Although this result was not expected based on the result from the first evaluation, the results in the validation phase correlates with the indications in the extended analysis regarding SVF and RHC made later on.

When analyzing SVF in section 5.1.3, it was noted that for the more critical temperatures, 5 to -5°C , the manually calculated SVF lead to higher errors. It was also discussed how the results from analyzing the hours during sunrise highlight the flaws of the manually calculated SVF. As described in section 3.2.2, it is critical that SVF is well calculated for sunrise and sunset since a poorly calculated SVF can create an offset in the timing of the sunrise or sunset. The effects on sunrise and sunset are confirmed by table 4.19, where the manually calculated SVF gives higher errors than default SVF.

When analyzing RHC from the evaluation phase, there are indications that a lower RHC could benefit the climate model for bicycle paths for colder temperatures. A lower value for RHC could also be a reason for why the default values are better than the modified in the validation phase. Note that the critical temperature interval and sunrise had not been analyzed when SVF and RHC were selected for the validation phase.

Although the errors for default parameters are generally lower, it is essential to highlight that the results for both combinations are concluded to be good, especially when taking into note that the tests are made during warmer months. That both modified and default gives good results, can be seen in the confusion matrices in figure 4.19b. In the confusion matrices, it can also be seen that the modified values reduce the number of false positives. At the same time, the accuracy of the overall model is better with the default values. However, it is difficult to determine what makes modified slightly better when it comes to false positives based on the results.

When comparing the results from Hede, seen in table 4.20, with the results from RWIS in table 4.21, it can be concluded that the default values do provide a good forecast, both for bicycle-paths and car-borne roads. Comparing Hede and RWIS, it can be seen that when using default values, the errors are of the same order of magnitude. However, the modified parameter values generate smaller errors for car-borne roads and higher errors for bicycle paths. This indicates that although the default values for bicycle paths are reasonable, there is a great potential to improve the model's performance and accuracy. It is therefore recommended to modify the climate model for bicycle paths further.

Based on the results, it is recommended to prioritize developing a method for calculated detailed SVF, similar to the method for car-borne roads. The second recommendation is to continue testing and tuning RHC, starting with lower RHC values for bicycle paths. The tuning of RHC is recommended to be carried out after a suitable method for SVF has been found. By first modifying SVF, consequential errors from having a poorly calculated SVF can be avoided when testing the RHC parameter. It can then become clearer which RHC is best suited for bicycle paths. It is also recommended to test the modification during the colder winter months, and on more massive data sets, to obtain more relevant results. Since the results when using default values are similar for both bicycle paths and car-borne roads, it is not considered to be necessary to investigate further the effect of Hede and RWIS measuring different weather data presented in table 4.2.

5.3 Evaluation of the method

By discussing the method used the possibility to create improved prerequisites for further projects regarding further development is possible. Overall the method was well developed, and the results generated from the method answer the research question and are in line with the aim of the project.

It was good to install Hede stations and examine the locations where Hede was installed since this resulted in gained knowledge about the positions and their specific microclimate properties. The Hede stations were well-positioned with a variation in microclimate. The variation in position and microclimate represented the reality and different circumstances for which the climate model will operate under. If they had been placed with the same conditions, it could have resulted in false securities and mislead the discussion. Note that more sensors providing more data and variation would have given better results, but four was a good amount given the time frame of the project. Something that could have facilitated the analysis of the results is to have the same knowledge about the location where the RWIS were placed. It would have been good to select RWIS with similar microclimates as the Hede stations to make a more in-depth analysis. However, in this project, it was prioritized to pick RWIS that were geographically close to the Hede stations and thereby had similar weather conditions. If the project had been rolled out for a more extended time, weather variations would have been more accepted, and microclimate could have been prioritized instead.

The climate model was modified and run through the software Docker, which worked well for the project. Although the set up of the software and the set up of the MySQL databases were more time consuming than expected, Docker and MySQL are concluded to be proper tools. The forecasts from Docker were compiled in CSV files, which made the output compatible with Matlab, which was a useful tool to use for compiling and analyzing the data.

It was considered to be beneficial to test the parameters individually. In retrospect, it would have been knowledgeable to test the parameters during the validation phase, both separately and combined. Another improvement would have been to perform the tests made in the phase on a data set consisting of a more extended period to get more reliable results. However, this could not be done because of the limited time for this project.

When analyzing the results from the validation phase and comparing these with those from the evaluation phase, it becomes apparent that it is relevant to analyze the temperature interval close to zero degrees. The temperature interval 5 to -5°C , selected in this project, was considered to be a good weigh-off between getting as close to zero as possible without losing to many data points. If a longer period of time is examined it could be interesting to analyze temperatures that are even closer to zero. If a narrow interval is examined it should be noted that there is a risk of missing out on greater errors. It should also be noted that it could be beneficial to analyze other temperature intervals depending on the purpose of the analysis.

In retrospect, it would have been an improvement to do a thorough analysis with weightings, such as critical temperature intervals and confusion matrices, in the first evaluation as well. The added tools with limited temperature or time interval, differences between highest and lowest error, and confusion matrices are concluded to be useful. With these tools, the performance of the climate model could be analyzed through different perspectives and based on what was considered critical, which gives a deeper understanding of the results. In this project, the extended analyses were added later on. It would have given a better direction for the validation phase to analyze the results from the perspective of what was considered critical from the beginning. If the analysis was done with the temperature interval 5 to -5°C from the beginning, the indications from these results could have been tested on the more extensive validation data set, and not only on the limited test data set. However, the validation phase results are still interesting, and it can not be concluded if another modification would have given more interesting results.

For future work, it is recommended to follow the structure of the method used in this project. Improvements that are recommended to implement are to test on more stations and test in a more significant period. A way to test on more considerable periods is to extend the test data set and to validate each parameter individually as well as validating them combined. Since there is a method for installing Hede stations, there is a possibility to expand the station network for bicycle paths, enabling testing on more stations. It is recommended to use data collected during the colder winter months, to get more relevant results. It is also recommended to add the extended analysis with limited temperature or time interval, differences between highest and lowest error, and confusion matrices, in the beginning, to get multiple perspectives from the start. To be able to distinguish differences between car-borne roads and bicycle paths in a more confident way, it is recommended to add analysis regarding the microclimates of all stations involved. It is also recommended to investigate why the measured values on the car-borne roads have lower temperatures. Another interesting analysis would have been to compare Hede stations and RWIS against an IR sensor, to see if how much they differ from a third independent source, and thereby examine further how good references Hede and RWIS are.

6

Conclusion and recommendations

This chapter presents the conclusions made for the Masters' thesis, Developing road temperature forecast to increase bicycle path safety as well as future work and recommendations. The project aimed to modify the RSI algorithm to predict the road temperature on bicycle paths, both around and in between stationary weather sensors, to improve road maintenance and ensure safer active transportation. To ensure the fulfillment of the aim, the following research question were formulated.

RQ.1 What are the differences between car-borne roads and bicycle paths, e.g., in terms of road construction and amount of traffic?

RQ.2 What modifications in the climate model lead to more accurate forecasts on an area surrounding Hede stations installed on bicycle paths, with measured data from the Hede stations as a reference?

RQ.3 Do the same modifications apply for car-borne roads with RWIS as a reference?

6.1 Conclusion

Regarding research question 1 (RQ.1), the differences between bicycle paths and car-borne roads were that bicycle paths had less traffic, less google street view information, fewer road construction restrictions, and no developed network collected data on bicycle paths. Also, it was found that the material of the surface might differ between car-borne roads and bicycle paths. These differences affected the parameters SVF, traffic amount, asphalt thickness, and road heat conductivity, which were modified for the climate model to answer research question 2. Since other stations were installed on the bicycle paths, it also affected what type of weather data that was collected, this did not seem to affect the climate model and was not reflected in the results. Aside from these differences, it can be seen in the measured values that the temperatures seem to be generally lower for car-borne roads, which has not been investigated further in this thesis. It should be noted that there are

other differences between bicycle paths and car-borne roads, which are not defined in this thesis.

Regarding research question 2 (RQ.2), the analysis from the first evaluation was lacking, leading to unexpected results from the validation. Because of the unexpected results, no conclusions regarding exactly which modifications in the climate model that lead to better performance for an area surrounding the stationary Hede stations could be drawn. However, conclusions regarding the significance of the different modifications could be drawn. It was found that modifying traffic amount and asphalt thickness did not affect the climate model much. The parameters that had a significant impact on the climate model were SVF and RHC. It should be noted that the results using default values on the parameters are concluded to be good for bicycle paths.

Regarding research question 3 (RQ.3), the parameters with a significant impact for bicycle-paths, are also significant for car-borne roads. However, when comparing the forecasts with RHC modified, it could be seen that the same modifications regarding RHC did not apply for car-borne roads and bicycle paths. There were indications that the accuracy increased for car-borne roads when high values on RHC was used, while it seemed like forecasts made on bicycle paths would benefit from using lower RHC values. When analyzing the forecasts where SVF was modified, it could be seen that the more precise method used to calculate SVF for car-borne roads generated better accuracy and performance for the climate model. Even though the method could not be tested on bicycle paths, there were indications that the method used for calculating SVF on car-borne roads would improve the bicycle path results as well. It could also be seen by analyzing the results from forecasts made on bicycle paths, that simplified calculations for SVF could lead to higher errors.

Based on the answers to the research questions, it is concluded that the parameters SVF and RHC affect the accuracy of the forecasts the most. The master's thesis concludes that the climate model for car-borne roads works well on bicycle paths in terms of accuracy. However, when comparing the results for bicycle paths with those for car-borne roads, it becomes apparent that the climate model can be improved for bicycle paths. The measures to be taken depend on which temperatures are considered critical and the accuracy required for bicycle paths. Overall, based on the results, it is recommended to develop a better method for calculating SVF for bicycle paths and to test lower values for RHC on bicycle paths. The results generated in this project are considered to fulfill the aim and can be used to answer the research questions. Further work is needed to answer the research questions with more certainty,

6.2 Future work and recommendations

For future work, it is recommended to prioritize developing a method for calculated detailed SVF, similar to the method for car-borne roads. After a good method for calculating SVF has been found, it is recommended to continue testing and

tuning RHC, starting with lower RHC values for bicycle paths. By first modifying SVF, consequential errors from having a poorly calculated SVF can be avoided when testing and tuning the RHC parameter. It is also recommended to test the modification during the colder winter months, and on larger data sets, to obtain more relevant results. It is recommended to expand the station network for bicycle paths, following the installation process described in this thesis, to obtain more data for testing and validation.

Since the results of using default values are similar for both bicycle paths and car-borne roads, it is not necessary to further investigate the effect of Hede and RWIS measuring different weather data presented in table 4.2. It is not recommended to prioritize the testing and tuning of traffic amount or asphalt thickness since these parameters do not have a significant impact on the climate model.

It is recommended to add the extended analysis by analyzing the critical temperatures and time intervals, differences between highest and lowest error, and confusion matrices to get multiple perspectives throughout the analysis. To be able to distinguish differences between car-borne roads and bicycle paths in a more certain way, it is recommended to add analysis regarding the microclimates of all stations involved. It is also recommended to investigate why the measured values for the stations on the car-borne roads have lower temperatures. Another interesting analysis would have been to compare Hede stations and RWIS against an IR sensor, to see if how much they differ from a third independent source.

References

Almkvist, E. (2020, February 7). *Personal communication*.

Crevier, L.-P., & Delage, Y. (2001, May). *Metro: A new model for road-condition forecasting in Canada* (Vol. 40). Dorval, Quebec, Canada: Recherche en Prévision Numérique, Meteorological Service of Canada. Retrieved from <https://journals.ametsoc.org/doi/pdf/10.1175/1520-0450%282001%29040%3C2026%3AMANMFR%3E2.0.CO%3B2>

Data School. (2014). *Simple guide to confusion matrix terminology*. Retrieved from <https://www.dataschool.io/simple-guide-to-confusion-matrix-terminology>

Davéus, A. (2016). *Urbana mikroklimat i samband med förtätning: Strategier för gestaltning av urbana miljöer* (Master's thesis, SLU Alnarp, Landscape architecture). Retrieved from https://stud.epsilon.slu.se/9723/1/daveus_a_161128.pdf

Dirksen, M., Ronda, R., Theeuwesc, N., & Pagania, G. (2019, December). *Sky view factor calculations and its application in urban heat island studies*. Elsevier. Retrieved from <https://www.sciencedirect.com/science/article/pii/S2212095519300604>

European Commission. (2020). *Goal 11. make cities and human settlements inclusive, safe, resilient and sustainable*. Retrieved from https://ec.europa.eu/sustainable-development/goal11_en

Faskunger, J. (2008). *Aktiv transport: På väg mot bättre förutsättningar för gång- och cykeltrafik*. Folkhälsomyndigheten. Retrieved from https://www.folkhalsomyndigheten.se/contentassets/9621865e6bbc4d2c94ea689596bc73e3/r200831_aktiv_transport_08111.pdf

Geiger, R., Aron, R. H., & Todhunter, P. (1995). *The climate near the ground* (Fifth ed.). Braunschweig: Vieweg.

Gustafsson, O. (2019, December). *'cykelbokslut för jönköping 2018*. Jönköping Kommun. Retrieved from <https://www.jonkoping.se/download/18>

.39b0b26216eef970910626c/1576832358798/Cykelbokslut%202018.pdf

Gustavsson, T. (2020, March 16). *Peronal communcation*.

Hedström, R. (2013). Cykling och gående vid större vägar:några aspekter på anläggning, drift och underhåll samt kostnader för gc-lösningar vid större vägar. *VTI(777)*. Retrieved from http://fudinfo.trafikverket.se/fudinfoexternwebb/Publikationer/Publikationer_001801_001900/Publikation_001874/Delrapport%204%20VTI%20rapport%20777_2013_DoU_delrapport_CoG%20vid%20st%C3%B6rre%20v%C3%A4gar.pdf

Holst, S. (2020, March 10). *Personal communication*.

JJ. (2020). *Mae and rmse - which metric is better?* Retrieved from <https://medium.com/human-in-a-machine-world/mae-and-rmse-which-metric-is-better-e60ac3bde13d>

Klimator AB. (2020). *Product information*. Retrieved from <https://www.klimator.se/product>

Lindqvist, S., Mattson, J.-O., et al. (1983). *Vägklimatologi*. *TU(151)*.

Mayer, N. (2020). *Climat ou météo, quelle différence?* Retrieved from <https://www.futura-sciences.com/planete/questions-reponses/meteorologie-climat-meteo-difference-5922/>

Metlink. (2020). *Microclimates*. Retrieved from <https://www.metlink.org/secondary/key-stage-4/microclimates/>

Peterson, B., & Ringström, G. (1977). *Halkrisker vid olika väderlek och lokalklimat*. *TV(136)*.

SMHI. (2020). *Olika sorters strålning*. Retrieved from <https://www.smhi.se/kunskapsbanken/meteorologi/olika-sorters-stralning-1.5930>

Trafikverket. (2011, June). *Trvk väg:trafikverkets tekniska krav vägkonstruktion*. *TRV(2011:072)*. Retrieved from https://trafikverket.ineko.se/Files/sv-SE/10750/RelatedFiles/2011_072_TRVK_vag_2.pdf

Trafikverket. (2020, Mars). *Dataproduktspecifikation: Årsmedeldygnstrafik (Ådt) på statliga bilvägar mätt med mobil utrustning*. Retrieved from https://www.trafikverket.se/TrvSeFiler/Dataproduktspecifikationer/V%C3%A4gtrafikdataprodukter/Kvalitetsdeklaration_ADT.pdf

United Nations. (2020). *Envision 2030 goal 11: Sustainable cities and communities*. Retrieved from <https://www.un.org/development/desa/disabilities/envision2030-goal11.html>

Wågberg, L.-G. (2013). Val av beläggning. In T. Jacobson (Ed.), *Asfaltsbo-*

ken. Statens Väginstitut. Retrieved from <http://www.asfaltboken.se/val-av-belagging/>

A

Appendix 1

```
function table = load_forecast(totTime,n,folder)
%-----
% FUNCTION NAME:
% load_forecast
%
% DESCRIPTION:
%   A function extracting forecasts from csv files
%   created by the climate model. The function was
%   constructed to extract forecasts from csv files
%   produced from a climate model in the master's thesis
%   'Developing road temperature forecast to increase
%   bicycle path safety' conducted in spring 2020.
%
% ASSUMPTIONS:
%   - The climate model has been run once every hour.
%   - The folder contains csv files that are output
%     from the climate model.
%   - The folder name is the same as the endings of
%     the csv files in the folder.
%
% INPUTS:
%   - totTime: (datetime vector) A datetime vector with
%     the start- and end date and time for the desired
%     forecast. The time step in the vector is one hour.
%
%   - n: (integer) The forecast time, i.e., how far ahead
%     in time the forecast predicts. n is a number between
%     0 and 18. A forecast made n hours ahead in time is
%     called the n-hour forecast.
%
%   - folder: (directory) Which folder that should be
%     analyzed. The folder name should be the parameter
%     value and represent each modified parameter and its
%     value. Each csv in the folder should be named after
```

A. Appendix 1

```
% which time the climate model has been run, which
% parameter that has been modified, and the value of
% the modified parameter, following the pattern
% yyMMdd_HH_parametervalue.csv. yyMMdd_HH represent
% the date and time for which the climate model has
% been run, and parametervalue represent which
% parameter that has been modified and its value.
% For an example, if the climate model had been run
% for 27 feb 08:00, with default parameters, the name
% of the csv file should be 200227_08_def.csv.
% Observe that the ending of the csv file and the
% folder name should be the same i.e.,
% foldername = parametervalue.
%
% OUTPUT:
% - table: (table) A table containg the forecasts for
% all Hede and RWIS stations from all date and times
% in vector totTime.
%
% REVISION: Matlab R2019a
% AUTHOR: Tina Mostafavi
% DATE: April, 2020
%-----

% Findind name of folder
[~,foldername]=fileparts(folder(end).folder);

% Creating filenames for files from n hours before
% forecast start, to n hours before forecast end.
% The purpose is to filter out the files that the
% function needs to go through
totTime_str=totTime-hours(n);
totTime_str.Format='yyMMdd_HH';
totTime_str=string(totTime_str);
filenames_filter=strcat(totTime_str,'_',foldername,...
'.csv');

%All files in the folder
filenames_all={folder.name};

% Filtering out the files from n hours before start time
% until n hours before end time
files=ismember(filenames_all,filenames_filter);
filenames=filenames_all(files);
% Prints an error message if the size of the datetime
% vector totTime doesnot match the number of files
```

```

% filtered out
if size(filenamees,2) ~=size(totTime,2)
    fprintf('Error! Number of hours (%d) and files (%d)
        did not match. Some files might have wrong
        filenamees or might be missing in %s.\n',...
            size(totTime,2),size(filenamees,2),string(folder(
                end).folder))
end

% Preallocating
table=[];
% Loop that goes through every file from n hours before
% start time of the forecast until n hours before end
% time, and extract the rows that has the same date
% and time as totTime, i.e., extracts the n-hour
% forecasts
for i=1:1:size(filenamees,2)
    % Filepath
    s2=filenamees(i);
    s=string(strcat(folder(end).folder,'\ ',s2));
    % Reading table
    tab_tmp=readtable(s);
    % Prints error message if the the row that should
    % correspond to the datetime in totTime, does not
    % match.
    if tab_tmp.DateTime(1+n) ~=totTime(i)
        fprintf('Error! %s in %s did not load properly. %s
            might contain the wrong forecasts.\n',...
                string(totTime(i)),string(s2),string(s2))
    end

    % Picking out the rows with the same date and times
    % as
    % in totTime
    dates=ismember(tab_tmp.DateTime, totTime(i));
    tab_tmp=tab_tmp(dates,:);
    % Storing the rows in the final table
    table=[table;tab_tmp];
end

% Converting the table to timetable
table=table2timetable(table);
% Removes segment 7 that corresponds to RWIS 611,
% that was not used in the project
table(7==table.Segment,:)=[];

```

A. Appendix 1

```
% Prints error message if any surface temperature in
% the final table is equal to -9999.9, since this
% indicated that the climate model did not run
% properly
if any(ismember(table.SurfTemp,-9999.9)==1)
    rows=find(table.SurfTemp==-9999.9);
    fprintf('Error! Some surface temperatures has
           resulted in -9999.9. Check rows ');
    fprintf('%g ', rows);
    fprintf('\n');
end

end
```